AECL--10370

CA9200233

AECL-10370

ATOMIC ENERGY OF CANADA LIMITED

ÉNERGIE ATOMIQUE DU CANADA LIMITÉE

FRACTURE DETECTION AND GROUNDWATER FLOW CHARACTERIZATION IN POORLY EXPOSED GROUND USING HELIUM AND RADON IN SOIL GASES

LA DÉTECTION DES FRACTURES ET LA CARACTÉRISATION DE L'ÉCOULEMENT DES EAUX SOUTERRAINES EN SOL MAL À DÉCOUVERT À L'AIDE DE L'HÉLIUM ET DU RADON FAISANT PARTIE DES GAZ DU SOL

M. Gascoyne, D. M. Wuschke

Whiteshell Laboratories Laboratoires de Whiteshell
Pinawa, Manitoba R0E 1L0
May 1991 mai

AECL RESEARCH

FRACTURE DETECTION AND GROUNDWATER FLOW CHARACTERIZATION IN POORLY EXPOSED GROUND USING HELIUM AND RADON IN SOIL GASES

Final Report
for the Joint UKDOE/AECL/USDOE Project

by

M. Gascoyne* and D.M. Wuschke**

* Applied Geoscience Branch
**Environmental and Safety Assessment Branch

Whiteshell Laboratories
Pinawa, Manitoba R0E 1L0
1991

AECL-10370

LA DÉTECTION DES FRACTURES ET LA CARACTÉRISATION DE L'ÉCOULEMENT DES EAUX SOUTERRAINES EN SOL MAL À DÉCOUVERT À L'AIDE DE L'HÉLIUM ET DU RADON FAISANT PARTIE DES GAZ DU SOL

par

M. Gascoyne et D.M. Wuschke

RÉSUMÉ

On s'est servi du radon et de l'hélium faisant partie des gaz du sol pour identifier les points de déversement d'eaux souterraines et la présence de fractures affleurant au-dessous des morts-terrains dans deux aires situées près du Laboratoire de Recherches Souterrain (LRS), à Lac du Bonnet, Manitoba, Canada. On a nettement identifié, en particulier, le déversement d'eaux souterraines d'une zone de fractures inclinée, connue, du LRS par un surplus d'hélium constaté dans les gaz du sol surjacent. On a réalisé un modèle afin de décrire l'écoulement du gaz non dissout dans la roche de fond et les morts-terrains de cet endroit, à partir d'une injection de gaz dans un trou de forage adjacent. On a prédit la voie de migration du gaz et le temps de passage du gaz à la surface, en vue d'un essai d'injection de gaz.

EACL Recherche
Laboratoires de Whiteshell
Pinawa (Manitoba) ROE 1LO
1991

AECL-10370

FRACTURE DETECTION AND GROUNDWATER FLOW CHARACTERIZATION IN POORLY EXPOSED GROUND USING HELIUM AND RADON IN SOIL GASES

by

M. Gascoyne and D.M. Wuschke

ABSTRACT

Radon and helium in soil gases have been used to identify locations of groundwater discharge and the presence of fractures outcropping beneath overburden in two areas near the Underground Research Laboratory (URL), Lac du Bonnet, Manitoba, Canada. In particular, groundwater discharge from a known, inclined fracture zone at the URL was clearly identified by a helium excess in overlying soil gases. A model was developed to describe gas phase flow in bedrock and overburden at this location, from gas injection in an adjacent borehole. Predictions were made of gas transport pathway and breakthrough time at the surface, in preparation for a gas injection test.

AECL Research
Whiteshell Laboratories
Pinawa, Manitoba R0E 1L0
1991

AECL-10370

CONTENTS

continued...

CONTENTS (concluded)

EXECUTIVE SUMMARY

Soil gas sampling and analysis have been performed in two sections of the Underground Research Laboratory (URL) lease area, near Lac du Bonnet, Manitoba, Canada. This work had two main goals: 1) to test the suitability of using radon and helium in soil gases as indicators of the local hydrogeology and of subsurface bedrock fracturing; and 2) to develop a model for gas flow, from an injection borehole to the surface, through a permeable fracture zone in the study area.

One of the two sections studied is an upland bush and marsh area, thought to be a region of recharge for deep subhorizontal fracture zones detected in boreholes on the URL lease area. The other section is a lower-lying, flat field between the Lee River and the URL, believed to be an area of discharge for one of these fracture zones (Fracture Zone 2, FZ2). In each area, the overburden is of a type new to the application of this technique.

Locations of high Rn and He concentration in soil gases were found in both study areas when sampled on a 50-m interval grid, with concentrations ranging from 500 to 6000 pCi*/L Rn and -100 to +500 ppb** He (relative to atmospheric He concentrations). In the recharge area, the high-He locations were very limited in extent and lay within the broader areas of high Rn concentration. The distribution of anomalous concentrations of both gases bears little relation to local hydrogeology. Sediment type, thickness and ^{226}Ra content are probably more important in controlling Rn levels and flux.

In the discharge area, a pronounced He excess was found near the suspected subcrop location of FZ2. A more detailed survey of Rn levels in a 100-m square section within the He anomaly in the discharge area found two sites of exceptionally high Rn content. Although the scales of the He and Rn surveys differ considerably, this result suggests that the localized Rn anomalies indicate the areas of most rapid groundwater discharge from the underlying fracture zone, whereas the broad helium anomaly delineates the total region of groundwater discharge. A 10-m interval grid was found to be the optimum size for a survey where highly variable results might be expected. The soil gas radon content showed no correlation with elevation of the sample site, water and Ra content of the sampled horizon in the discharge area. It appears, therefore, that the high-Rn anomalies are due to groundwater discharge alone.

Dissolved He and Rn contents have also been determined for groundwaters from boreholes penetrating FZ2 to examine the variation in concentration of these gases in groundwater between recharge and discharge areas. Radon and He concentrations range from <1 to 50 nCi/L and 1 to 56 cm^3 STP/L respectively. High Rn levels occurring in recharge groundwaters that enter FZ2 through vertical fractures in the bedrock are probably due to Ra enrichment in fracture wall coatings. In the discharge area of FZ2, high Rn concentrations in groundwater are probably due to local recharge through vertical

---

* 1 Ci = 37 GBq
**1 ppb = 1 nL/L

fractures that intersect the near-surface portion of FZ2. High He levels are also found in vertical fractures that occur between the recharge and discharge areas, but He is relatively low in deep groundwater in the recharge area. Slow groundwater discharge to surficial sediments appears to be occurring with added localized groundwater circulation that dilutes salinity and He content while increasing Rn content. These results fit the model of Gregory and Durrance (1987).

In preparation for Phase 2 of the project, a gas injection test, a model has been developed to describe the movement of a gas phase in a permeable water-saturated fracture zone. Using the soil gas survey results and existing geological and hydrogeological information at the URL, model parameters have been defined for the injection of helium into a borehole in the discharge area. The borehole intersects FZ2 at a depth of about 40 m and the gas flow path along the fracture zone is approximately 120 m.

The model has been applied to two situations: 1) flow to the surface through bedrock fractures for the entire distance assuming no overburden cover, and 2) flow in the fracture plane to the base of the overburden and then vertical flow through 13 m of fractured clay overburden having a permeability three orders of magnitude lower than the bedrock fracture zone.

The model calculates required injection pressures, and breakthrough times at the surface. Predicted breakthrough times are all less than one day. If allowance is made for excess porosity in the flow path, these times increase to about three to eight days for injection pressures of 0.4 to 0.5 MPa.

This work was performed and jointly funded as part of an agreement between AECL and the U.K. Department of the Environment. This report was initially published in limited quantities as UKDOE Report No. DOE/RW/90/079. The results of this work will be used in the formulation of U.K. Government Policy but views expressed in this report do not necessarily represent U.K. Government Policy.

1. INTRODUCTION

Helium and ^{222}Rn (here referred to as radon) are the main gases produced in the subsurface as a product of radioactive decay of U- and Th-bearing minerals. Helium is stable and accumulates with time, whereas Rn has a 3.8-d half-life and reaches a constant concentration in a closed system containing ^{226}Ra. Both gases tend to diffuse out of their host minerals and, because of their solubility, accumulate in groundwater. In plutonic rocks, groundwater flow occurs almost exclusively along fractures and extremely high levels of He and Rn have been observed in groundwaters at depth, especially in U- and Th-rich plutonic rocks (Andrews et al. 1980, Bottomley et al. 1984). Depending on flow conditions, both gases will tend to diffuse upward to the atmosphere where the fractures outcrop at the surface. In a groundwater recharge situation, the upflow of gases is limited, but in a discharge environment high-concentration flows of He and Rn enter the atmosphere or mix with soil gases if the fracture outcrop is covered by sediments. The relative level of Rn that can be found at shallow depths in the overburden depends largely on groundwater velocity rate, because Rn concentrations decline rapidly with time of travel away from the source.

These principles have led to the use of gases in soil and shallow groundwater as a method of detecting subsurface bedrock fractures and for determining local hydrogeological conditions (Larocque and Gascoyne 1986, Gregory and Durrance 1987, Banwell and Parizek 1988). This report describes work done for Phase 1 of the joint UKDOE/AECL/USDOE project to investigate He and Rn abundances in groundwater and soil gases in two distinct hydrogeological regimes (recharge and discharge), for a fractured Archean granite partly covered by Quaternary sediments. This study differs from previous applications in that the overburden type is dominantly clay, and the vegetative cover varies from bare cropland to a dense low bush with timber deadfall. The measurements are related to the known hydrogeological and geological features in the areas, and are used to verify the application of soil gases as a characterization tool in site investigation studies, and to develop a model for describing gas phase flow in a water-saturated fracture zone in the granite and overburden cover.

2. HELIUM AND RADON IN SOIL GASES AND GROUNDWATERS

2.1 AREA DESCRIPTION

The study was carried out in the Whiteshell Research Area, on the western portion of the Lac du Bonnet granite batholith, in southeastern Manitoba (Figure 1). The granite is Archean in age (~2600 Ma) and forms part of the English River gneiss belt, within the Superior Structural Province, at the western margin of the Canadian Shield.

Soil gas sampling was performed in two areas in, and adjacent to, the Underground Research Laboratory (URL) lease (Figure 2). The upland area, covered by low bushes, tree stands and marshes (known as the East Swamp), is believed to be a region of groundwater recharge to a deep, inclined

fracture zone observed in URL boreholes. The fracture zone, known as Fracture Zone 2 (FZ2), is about 350 to 450 m deep in the vicinity of the East Swamp. The other area, a lower, flat-lying crop field near the Lee River is a region of groundwater discharge from this fracture zone. Overburden thickness is between about 5 and 30 m, and the fracture zone subcrops immediately beneath the overburden in the discharge area. A simplified representation of the hydrogeological relationship between the two areas is shown in Figure 3. Overburden type and thickness in the recharge area have been determined by Killey and Munch (1990) and a summary of overburden thickness is shown in Figure 4. Some data on the overburden in the discharge area have been obtained by drilling during Phase 2 of the soil gas project (Gascoyne 1990).

Sampling of gases dissolved in groundwaters has been done mainly in boreholes in the URL lease area. Over 130 boreholes have been drilled from ground surface to characterize the subsurface geological and hydrogeological conditions. From this work, three subhorizontal fracture zones have been identified in the upper 500 m of rock at the URL (Davison 1984). FZ2 is the most extensive fracture zone in the lease area and best characterized because it lies closest to the underground excavation.

Twenty boreholes that are collared at ground surface intersect FZ2 (some are shown in Figure 3). Over thirty more, drilled from the 240-m level of the URL also intersect FZ2. Hydrogeological testing of FZ2 has shown that the zone contains regions with hydraulic conductivities varying by over six orders of magnitude (from $>10^{-4}$ to $<10^{-10}$ m/s) over distances of a few metres (Davison and Kozak 1988). Well-defined patterns of high and low permeability exist and the high-permeability regions are often connected to form dendritic channels. In addition, isolated pockets of high permeability are also found within larger regions of low permeability.

Prior to excavation of the URL shaft in 1984, groundwater moved up the dip of FZ2 from a region of deep recharge to the southeast (underlying the East Swamp) towards discharge at the surface in the northwest (the discharge region). Hydraulic and hydrochemical data indicate that relatively dilute groundwaters have penetrated to FZ2 from the surface beneath the East Swamp probably through a steeply inclined or vertical fracture set believed to exist in the recharge area.

Hydraulic pressure head data now indicate that, following shaft excavation and draining of Fracture Zone 3 (FZ3), FZ2 is no longer being recharged from this surface area, but, instead, discharges groundwater upwards to FZ3 along these fractures (Figure 3). A gradual change in groundwater composition and dissolved gas content is expected to occur in this area; however, because flow rates are very low, these changes are unlikely to have influenced the results of this study.

A variety of techniques has been used to determine the hydrogeological characteristics of FZ2, including single-borehole straddle packer tests and large-scale hydraulic-pressure interference testing. A full description of this work is given by Davison and Kozak (1988). The patterns of groundwater flow and permeability appear to be related to that of groundwater concentrations within the zone, in particular, chloride ion content. An example of the spatial variability of Cl content is shown in Figure 5.

These variations can be explained by a combination of rock-water interaction and mixing between dilute and saline groundwater bodies in various parts of the fracture zone (Gascoyne et al. 1988). It is possible that these factors also influence the dissolved gas content of groundwater in the area.

2.2 SAMPLING AND ANALYTICAL METHODS

Sampling of soil gases was initially performed over a 50-m interval grid in the discharge area and over a 50-m N-S interval and 200-m E-W interval grid in the recharge area. Sampling at more frequent intervals on an E-W grid in the latter area proved extremely difficult because of the presence of deadfall and low dense bushes. Only a few closer-spaced intervals were sampled in this area. Overburden groundwaters were also sampled from 17 multi-level piezometers installed throughout the recharge area (Killey and Munch 1990). In a second study, a more detailed sampling of soil gases (at 10-m intervals) was performed in a section of the discharge area 110 m ESE x 100 m SSW (Figure 2) to better define anomalous patterns of gas concentration in the discharge area.

Samples of soil gas were obtained by driving a hollow stainless steel probe into the overburden to a depth of 0.5 ± 0.05 m, connecting a manifold assembly to the probe outlet and drawing soil gas into the assembly using a hand pump. A full description of the procedure is given in Appendix A. The Rn content of soil gases was determined by scintillation counting in a calibrated Lucas cell and He abundance was analysed using a modified Veeco helium-leak detector. Both methods are described in Appendix A. Helium analysis of soil gas samples was not performed in the second part of the study, which involved detailed sampling of the discharge area, because of poor analytical precision and instability of the Veeco instrument. Therefore, only Rn concentration was determined in this part of the study.

Sampling of dissolved gases in shallow groundwater in multi-level piezometers in the East Swamp recharge area was performed using a battery-operated peristaltic pump (Appendix A). Sampling of dissolved gases in groundwater from surface boreholes penetrating FZ2 was performed using a downhole bladder pump driven by compressed air or bottled nitrogen. Dissolved gases in groundwater in the underground boreholes at the 240-m level in the URL facility were readily sampled by opening valves that access the isolated part of the fracture zone. The ambient hydrostatic pressure (about 2000 kPa) forced the groundwater into collection vessels under pressure, without pumping. In all sampling situations, samples were collected in flow-through stainless steel vessels (fitted with Nupro valves) that were well flushed to remove air.

Helium was extracted from groundwater samples on an evacuated line fitted with cold traps and then analysed by a CEC (DuPont) 21-130 voltage-scanning, gas-source mass spectrometer. Radon was initially determined by the Lucas cell method, but a liquid scintillation technique, subsequently developed and used, was found to give greater precision and accuracy.

A topographic survey and soil sampling program was conducted in conjunction with the detailed study of soil gases in the discharge area to determine if a relationship existed between soil gas Rn content and elevation, moisture

content and ^{226}Ra concentration in the soils. Sampling and analytical details are given in Appendix A.

2.3 CONTROLS AND ANALYTICAL PRECISION

The variation in He and Rn content of soil gas due to daily variations in barometric pressure were monitored by regular sampling of two permanently installed soil probes, one in each area. In addition, for the initial part of the study, about 20 sites in the East Swamp area were sampled for Rn at least twice. Calibration of the He measurement technique was done by checking for a linear response in the analysis of air (5.24 ppm* He) and two He standards in N_2 gas (10 and 20 ppm). Estimation of the measurement precision for each gas has been done in three ways: 1) analysis of duplicates for each sampling site (mainly for He), 2) replicate sampling of a number of locations on different occasions (mainly for Rn), and 3) repeated analysis for Rn, on a daily basis, of soil gas samples from two "standard" sites.

The reproducibility of the He analysis is mainly affected by stability of the mass spectrometer chart signal (see Appendix A). This error is estimated to be about ±50 ppb** He, based on observed fluctuations in He content for each pair of samples taken at a sampling site. Duplicate samples for Rn analysis for the same site were taken in the preliminary determination of number of pump strokes to remove trapped air during sampling, and results were found to be reproducible to within ±3%. Daily variations in barometric pressure induced larger changes in radon level (Table 1) and ranges between ±5 and ±15% for the two standard sites. The same range is expected to apply to daily variations in He content. No corrections for barometric pressure effects were made to the Rn and He results from the first part of the study. In the more detailed study of soil gases in a section of the discharge area, the variation in Rn content of soil gas due to barometric pressure was monitored by sampling the standard site before and immediately after each day's sampling session. Daily variations in barometric pressure caused changes in Rn levels of up to 25% during the three-week sampling period. To correct for this effect, a reference value for the Rn content at the standard site was arbitrarily chosen and was the value for one day when barometric pressure was 101.3 kPa in Winnipeg. The two values obtained for the standard site during a day's sampling were averaged and the difference between this value and the reference value was used to normalize all the results for that day.

Anomalous features in the detailed study were resampled to check for authenticity and sites at a 2.5-m interval within parts of the grid were also sampled. All features found on the 10-m grid were confirmed on the denser grid and all features on the 2.5-m grid were found on the larger grid.

---

* 1 ppm = 1 µL/L
** 1 ppb = 1 nL/L

2.4 RESULTS

2.4.1 Soil Gas Surveys

Variations in Rn and He concentrations for soil gas in the recharge and discharge areas are shown in Figures 6 and 7 and the data are listed in Table 1. Concentrations of Rn in groundwaters from the piezometers in the recharge area are given in Table 2.

Several regions of elevated Rn and He levels in soil gas can be seen in both of the study areas; these regions do not always overlap. The overburden groundwater Rn results are more difficult to interpret because they probably do not fully represent the ambient concentration in the piezometer zone (see Appendix A), and the piezometers are more widely separated than the soil gas samples.

A list of normalized Rn concentrations and the sample site coordinates for the detailed survey of the discharge area is given in Table 3. Variations in Rn concentrations of soil gas in the study area are shown as a contour map in Figure 8. Maximum Rn concentration exceeds 6000 pCi*/L at coordinate 2-8 (Table 3). Distinct high- and low-concentration features are apparent in Figure 8. Both the topographic survey of the section in the discharge area and the analyses of soil samples showed that no significant relationship exists between Rn concentration and ground elevation (Figure 9), water content (Figure 10), or ^{226}Ra content of the soil (Figure 11).

2.4.2 Groundwater Analyses

Concentrations of He and Rn in groundwaters in FZ2 and adjacent vertical fractures are summarized in Table 4. Results for surface boreholes in the URL lease area are shown in the upper part of the table and data from the underground boreholes (the HC-series for FZ2 and horizontal boreholes that intersect vertical fractures at the 240-m level in the URL) are presented in the lower parts. These results are shown in plan view in Figures 12 and 13, for the lease area and 240-m level (FZ2) groundwater respectively. The relationship between dissolved He and Rn content is shown in Figure 14 for samples where both analyses have been made.

2.5 DISCUSSION

2.5.1 Soil Gas Concentrations

Concentrations of soil gas Rn in the recharge area are generally greater than in the discharge area (Figure 6a and 7a), and range from >500 to 9600 pCi/L (recharge) and 500 to 4300 pCi/L (discharge). Conversely, He concentrations tend to be higher in the discharge area (up to 530 ppb above air levels), especially at locations close to the road and to borehole B34 (Figures 6b and 7b). The one location in the recharge area where high He levels occur (up to 400 ppb above air) is small and tends to be isolated,

---

* 1 Ci = 37 GBq

unlike the broader enrichment seen in the discharge area. Resampling of one of these sites twice in the recharge area verified the He anomaly, but found somewhat lower values (+160 and +200 ppb).

These levels of He, particularly those in the discharge area, are some of the highest reported for unmineralized bedrock (Gregory and Durrance 1987, Banwell and Parizek 1988) and are probably due to a combination of several factors: 1) the abundance of He in the U- and Th-enriched Archean granite, 2) the presence of active weathering and alteration zones associated with bedrock fractures, and 3) the well-defined hydrogeological flow system known to bring saline groundwater to the surface in the discharge area (Gascoyne et al. 1987).

In general, negative helium values tend to be more prevalent in the recharge area (Table 1). This can be explained by the greater saturation of the overburden by water in this area, a characteristic that has been shown to depress He levels in soil gas below atmospheric values (Hinkle and Ryder 1987).

High Rn concentrations in soil gases in the recharge area appear to be distributed in a pattern unrelated to any bedrock structural control found in the area. It is more likely that areas of high Rn concentrations in the recharge area are due to sediment type and Ra content (the Lake Agassiz clay unit outcrops at the surface where Rn concentrations are highest). Recent hydraulic head measurements from piezometers in the area (Killey and Munch 1990) have indicated that low permeabilities of overburden sediments limit the groundwater flow velocities to a few metres per year, at the most. Hydrogeological factors are unlikely, therefore, to control soil gas Rn levels. The one location with high He (Station 3-16, Table 1) in the recharge area may indicate subsurface bedrock fracturing coupled with a local upflow condition.

In the discharge area, the clear broad band of He enrichment in soil gases to the NW of the road indicates groundwater discharge from underlying fractures at this location. Although FZ2 is known to be about 40 m deep in the vicinity of B34, vertical fracturing is suspected to intersect the zone in this area and could provide discharge pathways for groundwater and dissolved gases. The NE-SW orientation of He enrichments is consistent with the strike of FZ2 and the orientation of vertical fractures seen nearby in outcrops. The occurrence of two locations of high Rn levels (up to 4300 pCi/L) along strike to the N and NE of the main He-enrichment area may indicate that discharge is more rapid here, thereby lessening the effect of Rn decay. Alternatively, the Rn could be derived from localized Ra enrichment caused by past precipitation from upwelling saline groundwater. The most active discharge zone at present is likely to be the area of high He and moderate Rn levels to the NW of the road.

Further definition of the discharge characteristics can be seen in the results of the detailed survey of the 100-m square section (Figure 8). Concentrations of Rn in soil gas in the sampled area range between 400 and 6400 pCi/L. In the previous survey of this section, Rn levels were found to range between 1400 and 2400 pCi/L (Table 1). This range falls within the span of results from the detailed survey but clearly misses the sites with high and low Rn levels.

Grid stations 2-8 and 3-8 (Figure 8) are 10 m apart and have isolated peak Rn levels of 6400 and 2600 pCi/L respectively. Sampling at 2.5-m intervals between them (Table 3) shows a decrease to about 800 pCi/L, giving a concentration gradient that exceeds 1000 pCi/(L·m). Resampling of the most extreme points was also performed in triplicate, confirming the two peaks as well as the low values between and around them. The area of the peaks is based on over 20 data points and therefore indicates some intense local feature. The grid area may be divided into two parts by a NE-SW line, with the southern part (uppermost in Figure 8), averaging 1400 pCi/L and the northern portion averaging 700 pCi/L. The NNE-SSW orientation of the line of peak Rn values is consistent with the strike of FZ2 in this area and the orientation of vertical fractures seen nearby in outcrops.

For the few soil samples analysed in the discharge area, ^{226}Ra concentrations in the soil were not found to correlate with soil gas radon levels (Figure 11). The ^{226}Ra content of the soil varies by less than a factor of three, compared with an order of magnitude variation in the Rn content in the soil gas samples. Calculations indicate that the ^{226}Ra measured in the soil would generate levels of radon that are between 0.6 and 25 times higher than the observed values if the system were closed and not open to the atmosphere. These observations suggest that the Rn is not only generated in situ, but a significant component may come from elsewhere. The broad features of the radon concentration surface may be caused by a general discharge of groundwater and the intensity of the gradients around the anomalies indicate the presence of channelling or localized higher velocity movement of the discharging groundwater in this area. Further investigations, such as drilling or the proposed injection of helium into FZ2, may help to verify this interpretation.

2.5.2 Groundwaters

Dissolved He concentrations vary widely (from 1 to 56 cm^3 STP/L) in FZ2 groundwaters (for reference, air-saturated water contains 4.75×10^{-5} cm^3 He/L at 10°C). Their distribution appears to bear little relation to location of the sample in the overall groundwater flow path (Figure 3). However, in the more detailed sampling at the URL 240-m level, more consistent values are found (~3-12 cm^3 STP/L) and lower concentrations tend to be observed in the most permeable parts of the zone. For instance, boreholes HC26-HC32 inclusive are each capable of discharging up to 500 L/min and those with He analyses indicate that He levels in that area tend to be relatively low (2.5 to 7.6 cm^3 STP/L). The high-permeability zone centred on HC7, 9 and 12 has higher associated He levels (6-11 cm^3 STP/L), but this is probably due to the fact that this zone is isolated and only receives restricted recharge. The two analyses of He content in groundwater from vertical fractures at the 240-m level (in boreholes PH3 and 209-0C1, Table 4) both show He to be relatively high. This may be due to dissolution from the rock (and, hence, a relatively long residence time) or diffusion upwards from FZ2 groundwater.

Radon exhibits considerably more variability in its abundance in FZ2 groundwater than He (<1-50 nCi/L). Because of its short life span, the ability of Rn to accumulate over time is severely limited, and therefore groundwater with a high Rn content is likely to be near the Ra source or to have flowed rapidly from the source location without incurring much decay.

Groundwaters in vertical fractures in boreholes from the 240-m level of the URL are enriched in Rn relative to groundwaters from the high-permeability parts of FZ2 (Table 4). The high Rn content of FZ2 groundwater from HC11, HC18, 209 and JE1 may indicate local recharge by known vertical fractures in the 209 area or recent (postglacial) deposition of Ra from solution in this location. In contrast, the FZ2 groundwater accessed by boreholes HC26-HC32 and in the HC9 area contains less Rn (1 to 10 nCi/L), which may reflect the greater distance from vertical fractures and/or the high water/rock ratio and well-leached nature of the bedrock in that area. (In earlier reports on this work (Gascoyne 1989), very low Rn concentrations were given for the FZ2 groundwaters. Resampling after discharge of larger volumes of water from the boreholes showed that the higher concentrations, now listed in Table 4, are more representative.)

2.6 CONCLUSIONS

The soil gas survey of He and Rn for two study areas adjacent to the URL lease area has shown anomalously high He and Rn concentrations in soil gases in both areas, which, in the discharge area, appear to correlate with the location of groundwater discharge from an extensive inclined fracture zone (FZ2) seen in boreholes at the URL. An area of significant He enrichment, covering approximately 100 m^2, defines the most active part of the discharge zone and, within this, a small area of high Rn concentrations may indicate the location of highest groundwater discharge. Elevation, soil moisture content and soil ^{226}Ra content appear to have little control over soil gas Rn level.

A single location in the recharge area with a verified He anomaly may indicate bedrock fracturing with localized upwelling, but, in general, low He values indicate bedrock recharge conditions. High Rn levels in this area are more likely to be due to overburden type and Ra content than bedrock fracturing, overburden thickness or hydrogeology.

The evolution of dissolved He and Rn concentrations in the inclined fracture zone (FZ2) at the URL does not conform to what might be expected from a simple conceptual model of recharge - fracture flow - discharge. Vertical fractures appear to readily contribute Rn to groundwater, probably because of Ra enrichment in fracture wall coatings, and these initial Rn levels are not sustained in the groundwater during flow in the fracture zone towards the discharge area. High Rn concentrations that are encountered in surface boreholes near the discharge area are probably a result of local recharge via vertical fractures to the near-surface portion of FZ2.

Dissolved He concentrations are high in groundwaters in vertical fractures that occur between the recharge and discharge areas. Limited available data suggest that He concentration is low in deep groundwater in the recharge area of the study and increases in a variable manner towards the discharge area. Dilution of the He content by different amounts of local recharge probably accounts for this variability. The dissolved gas data for groundwater in surface boreholes in the discharge area suggest that there is an inverse correlation of Rn with He. This may be interpreted with other available hydrochemical data to indicate that there is a fairly slow rate of discharge from FZ2 to surface sediments in the surveyed area,

with superimposition of a local groundwater circulation system that serves to dilute the salinity and He signatures while increasing that of Rn. This interpretation conforms to models proposed by Gregory and Durrance (1987).

3. MODEL DEVELOPMENT FOR A GAS INJECTION TEST

3.1 INTRODUCTION

The foregoing characterization of natural radon and helium abundances in soil gases and groundwaters has provided useful information on the hydrogeology and geochemistry of a recharge-to-discharge flow path in a granite of the Canadian Shield. In this situation, all gases are fully dissolved except where exsolution to the overlying sediments occurs in the discharge area, because of depressurization close to the water table. Movement of a discrete gas phase within saturated fractured rock is now examined by means of a gas injection test, in an attempt to better understand how gases evolving from an underground nuclear fuel waste disposal vault would migrate, and to determine if additional hydrogeological information may be obtained for an area when borehole data are unavailable.

For this part of the Phase 1 study, a simple analytical model has been developed to describe gas migration in fractured rock based on the flow regime and discharge location of FZ2 known from the location of the He anomaly described above and background geological and hydrogeological testing. The model uses experimentally determined bulk hydrogeological properties of the rock and overburden to provide estimates of

- the required threshold pressure for injection of He;
- the "breakthrough time", i.e., the time of initial arrival of the He at the surface, as a function of the injection pressure; and
- the velocity of the He after breakthrough, and its volumetric flow rate, as a function of injection pressure.

The derivation of the model equations, and a listing of parameter values are shown in Appendix B. The model is developed from previous work by Braester and Thunvik (1982) and Thunvik and Braester (1987). It describes the transport properties of a single open fracture and relates them to the bulk properties of the system by assuming an idealized fracture system.

Two sets of calculations were carried out: 1) for transport through a fracture zone with no overburden, and 2) for transport through a fracture zone with a low-permeability overburden. The two cases are described below.

3.2 TRANSPORT THROUGH A FRACTURE ZONE WITH NO OVERBURDEN

3.2.1 Conceptual Model

The injection test was conceptualized as shown in Figure 15. Helium gas is injected into FZ2 through borehole B34, 40 m below the surface. The permeability of the fracture zone is much greater than that of the surrounding rock, so transport outside the fracture zone is neglected. The

hydraulic conductivity of the fracture zone is 2 x 10^{-6} m/s, as determined by packer tests. The fracture zone is at an angle of 20° with the horizontal.

3.2.2 RESULTS AND DISCUSSION

The results of the calculations are shown in Table 5, Case 1. The required threshold pressure for gas injection is 0.39 MPa, essentially the hydrostatic pressure at 40 m, as capillary pressure is negligible.

Calculated breakthrough times as a function of the injection pressure are shown in Table 5 for injection pressures just exceeding the threshold pressure, and up to ~0.5 MPa. The breakthrough time is very sensitive to the amount by which the injection pressure exceeds the threshold pressure at low excess pressures, but becomes relatively insensitive at higher excess pressures.

There are large uncertainties in the calculation of the breakthrough times. The major uncertainty arises from the non-uniformity of fractures and the failure of the model to take this into account. Using a resin impregnation technique, Gale et al. (1987) and others have shown that non-uniform fractures have excess porosity that is not "seen" in packer tests, but would fill with gas during the transient. Gale et al. have shown that this porosity could be 100 times greater than the sampled porosity. Since the excess porosity is not taken into account in the model, the breakthrough times shown in the table could be underestimated by a factor of up to 100.

3.3 TRANSPORT THROUGH A FRACTURE ZONE WITH OVERBURDEN

3.3.1 Conceptual Model

In the location of the proposed gas injection zone (borehole B34 at the URL, Figure 2), the fracture zone is overlain by a fractured clay overburden that is 4 to 26 m thick and has lower permeability than the fracture zone. A variation of the above model was developed and calculations were carried out to take this into account.

For these calculations, the system was conceptualized as shown in Figure 16. Gas is injected into the fracture zone 40 m beneath the surface, as before, but, 13 m beneath the surface, the fractured rock is replaced by a low-permeability overburden. Flow through the overburden is assumed to be through vertical fractures; the path length is therefore considerably less than if the fracture zone continued to the surface.

No experimental data were available to define the properties of the overburden. Its hydraulic conductivity was estimated to be 1000 times lower than that of the fracture zone, and fracture spacing (d) was assumed to be one fracture per metre. This assumption is based on the fact that the overburden is known to be a fractured clay and the fractures are well spaced and form the main hydraulic pathways.

3.3.2 Results and Discussion

The results of these calculations are shown as Cases 2 and 3 in Table 5 for transport through the rock and overburden respectively. The threshold pressure for injection is essentially unchanged, since the hydrostatic pressure at the point of injection is unchanged and capillary pressures in both rock and overburden are nearly negligible in comparison. Breakthrough times for flow through the overburden are not very sensitive to the injection pressure over the range tested.

The total breakthrough time is the sum of the breakthrough times through the rock and overburden (i.e., Cases 2 and 3 in Table 5). For the case shown (d = 1 m), transport through the rock is much faster than through the overburden, and may be neglected, except at injection pressures just exceeding the threshold pressure. Breakthrough times through the overburden are decreased or increased by about a factor of four if the assumed fracture spacing is decreased or increased by a factor of ten. As in the case with no overburden, all breakthrough times may be up to 100 times greater than shown because of the time taken to fill excess porosity in non-uniform cracks. Additional uncertainties arise from the lack of information about the hydraulic conductivity and other properties of the overburden, the actual pathway of the gas, and the variable thickness of the overburden. Best estimates of the gas breakthrough time are from three to eight days for injection pressures of 0.4 to 0.5 MPa.

3.4 CONCLUSIONS

1. The injection tests must be carried out at a pressure exceeding the sum of the hydrostatic pressure and the highest capillary pressure along the flow path at the point of injection, i.e., at a pressure exceeding 0.4 MPa. The breakthrough time is insensitive to injection pressure, except when the latter is very close to the threshold pressure.

2. Transport of helium through the overburden is much slower than transport through the fractured rock. Hence, the breakthrough time is determined by the properties of the overburden.

3. There are very large uncertainties in the calculated breakthrough times because of lack of knowledge of the properties of the overburden and differences between the real system and the idealized system used to model it.

3. The "best estimate" of the breakthrough time is of the order of a few days, i.e., 10-20 times the sum of the breakthrough times given in columns 2 and 3 in Table 1, taking into account the excess porosity. Breakthrough times could be an additional one to two orders of magnitude higher or lower because of uncertainties in other parameters.

4. GENERAL DISCUSSION AND CONCLUSIONS

The analysis of Rn and He in soil gases in two areas adjacent to the URL has shown anomalies that may be correlated with (1) local lithology and Ra content (in the case of Rn) and (2) bedrock structure and groundwater movement (for He). The results obtained here generally support the model proposed by Gregory and Durrance (1987) in which locations of rapid groundwater discharge are denoted by high He and Rn levels in soil gases and slower groundwater discharges by high He and low Rn levels. Areas of groundwater recharge contain only atmospheric He with variable Rn levels. Examples of these features and the effect of flow through less radiogenic country rocks are shown in Figure 17.

The present study refines this model to some extent by showing the additional controls on Rn concentrations that may be imposed by overburden cover, especially if sediment permeabilities are low, thereby limiting the effect of local hydrogeology. In fact, because of the rapid radioactive decay of Rn, any bedrock derived Rn is likely to be difficult to observe in soil gases if the overburden is thick, of low permeability, or if groundwater discharge rates are not high.

This study has more clearly demonstrated the usefulness of He in soil gas as an indicator of subsurface fracturing and groundwater discharge. Levels of up to 0.5 ppm above atmospheric concentrations have been detected at sampling intervals of 50 m, covering an area approximately 150 m x 100 m. More detailed sampling within this area may reveal sites of greater concentration, as was observed for Rn content in the detailed 100 m x 100 m grid.

The results of the field sampling work generally support the premise that the recharge and discharge areas are aptly named, except that the hydraulic head measurements in the recharge area suggest that very little overburden groundwater recharges the bedrock flow system. Soil gas measurements of Rn and He do not distinguish between recharge to bedrock and lateral flow within overburden sediments. The importance of flow channelling and groundwater discharge through vertical fractures intersecting a near-surface, inclined fracture zone is clearly demonstrated, however.

The findings from the field characterization of the discharge area indicate that a gas injection test might be performed successfully in the discharge area, in borehole B34, which intersects the fracture zone (FZ2) at a depth of about 40 m. A model is developed here that describes gas phase flow through FZ2 to the surface considering initially no overburden and, subsequently, an overburden cover of about 13 m in depth. Helium is probably the best gas to use in the injection because it is inert, nonflammable and has a low solubility in water. It is also easy to detect in levels as low as 0.1 ppm above atmospheric concentrations. The existence of a natural He excess in the discharge area does not seriously compromise its use because over the short distance the gas is expected to migrate (~100 m), concentrations of He at the surface will likely rise to well over 1 ppm above background and so both gas breakthrough and peak concentrations will be readily determined.

The analytical model for gas phase flow indicates that the breakthrough time of gas at the surface depends on the gas overpressure, (i.e., the pressure in excess of hydrostatic pressure). The effect of gas overpressure is incorporated in the model and the calculated breakthrough time in the rock/overburden case ranges from 0.37 d for a slight overpressure of 3 kPa to 0.19 d for an overpressure of 103 kPa (Table 5).

The breakthrough time is also influenced by the excess porosity in non-uniform fractures. The available excess porosity is difficult to estimate because it is determined by the geometry of the fracture apertures, which depends on fracture zone permeability, porosity and tortuosity, and varies with distance along the flow path. As described in Section 3, estimates determined from resin impregnation tests suggest that breakthrough times may be up to 100 times greater than determined in field packer tests because of the time taken to fill excess porosity in non-uniform openings. A best estimate is proposed as being about 20 to 30 times greater than the calculated times. This results in an estimated breakthrough time of 7 to 11 d for slight overpressures of ~3 kPa. Because such small pressure differentials are difficult to measure and maintain in a gas injection test, it is likely that somewhat larger overpressures will be used, typically 10-30 kPa, therefore reducing breakthrough time to 3 to 8 d.

ACKNOWLEDGEMENTS

The field sampling and analytical work in this project has been performed mainly by Co-op Program students Ernest Wong and Martin Ridgway, with assistance from Andrew Stilling (Co-op student) and Rogan Watson (AECL). This report has benefitted from review by Dr. T. Chan and Dr. D. McConnell (AECL). Professor Eric M. Durrance (University of Exeter, U.K.) provided considerable assistance in initiating this work and in discussing the results.

REFERENCES

Andrews, J.N., I.S. Giles, R.L.F. Kay, D.J. Lee, J.K. Osmond, J.B. Cowart, P. Fritz, J.F. Barker and J. Gale. 1980. Radioelements, radiogenic helium and age relationships for groundwaters from the granites at Stripa. Geochimica Cosmochimica Acta 46, 1533-1543.

Banwell, G.M. and R.R. Parizek. 1988. Helium 4 and radon 222 concentrations in groundwater and soil gas as indicators of zones of fracture concentration in unexposed rock. Journal of Geophysical Research 93, 355-366.

Bottomley, D.J., J.D. Ross and W.B. Clark. 1984. Helium and neon isotope geochemistry of some groundwaters from the Canadian Precambrian Shield. Geochimica Cosmochimica Acta 48, 1973-1985.

Braester, C. and R. Thunvik. 1982. An analysis of the conditions of gas migration from a low-level radioactive waste repository. Swedish Nuclear Fuel Supply Co., Division KBS Report, SKBF-KBS-TR-83-21.

Davison, C.C. 1984. Monitoring hydrogeological conditions in fractured rock at the site of Canada's Underground Research Laboratory. Groundwater Monitoring Review, Fall issue, 95-102.

Davison, C.C. and E.T. Kozak. 1988. Hydrogeological characteristics of major fracture zones in a granite batholith of the Canadian Shield. In Proceedings of the 4th Canadian/American Conference on Hydrogeology (Hitchon, B. and Bachu, S. editors), Banff, AB, 1988, 52-59.

Gale, J., R. Macleod, J. Welhan, C. Cole and L. Vail. 1987. Hydrogeological characterization of the Stripa site. Swedish Nuclear Fuel and Waste Management Co. Report, KBS-SP-87-15.

Gascoyne, M. 1989. Fracture detection and groundwater flow characterization in poorly-exposed ground using helium and radon in soil gases. Interim Report on Activities for the Joint UKDOE/AECL/USDOE Project, AECL, Pinawa, Manitoba.

Gascoyne, M. 1990. Fracture detection and groundwater flow characterization in poorly-exposed ground using helium and radon in soil gases. Phase 2 Status Report for 1989 September-1990 February, AECL, Pinawa, Manitoba.

Gascoyne, M., C.C. Davison, J.D. Ross and R. Pearson. 1987. Saline groundwaters and brines in plutons in the Canadian Shield. In Saline Water and Gases in Crystalline Rocks (Fritz, P. and Frape, S.K., editors), Geological Association of Canada Special Publication No. 33, 53-68.

Gascoyne, M., J.D. Ross and R.L. Watson. 1988. Geochemical and isotopic characterization of flow in fractured rocks: Examples from the Canadian Shield. In Proceedings of the 4th Canadian/American Conference on Hydrogeology (Hitchon, B. and Bachu, S., editors), Banff, AB, 1988, 20-31.

Gregory, R.G. 1987. Soil gas emanometry and hydrothermal mineralization in southwest England. Unpublished PhD thesis, University of Exeter, Exeter, U.K.

Gregory, R.G. and E.M. Durrance. 1987. Helium, radon and hydrothermal circulation associated with the Carnmenellis radiothermal granite of southwest England. Journal of Geophysical Research 92 (B12), 12567-12586.

Hinkle, M.E. and J.L. Ryder. 1987. Effect of moisture and carbon dioxide on concentrations of helium in soils and soil gases. Journal of Geophysical Research 92, 12587-12594.

Killey, R.W.D. and J.H. Munch. 1991. Overburden/bedrock hydrogeology of the east margin of the URL site. Atomic Energy of Canada Limited Report, AECL-10166 (in preparation).

Larocque, J.P.A. and M. Gascoyne. 1986. A survey of the radioactivity of surface water and groundwater in the Atikokan area, northwestern Ontario. Atomic Energy of Canada Limited Technical Record, TR-379.*

Thunvik, R. and C. Braester. 1987. Calculation of gas migration in fractured rock. Swedish Nuclear Fuel and Waste Management Co. Technical Report, KBS-TR-87-18.

---

* Unpublished report available from SDDO, AECL Research, Chalk River Laboratories, Chalk River, Ontario K0J 1J0.

TABLE 1

Rn CONCENTRATIONS AND VARIATION OF He CONCENTRATION FROM THAT OF AIR FOR ALL SOIL GAS SAMPLE SITES. STATIONS D2-9 AND 2-18 ARE THE STANDARD SITES FOR REGULAR SAMPLING IN THE DISCHARGE AND RECHARGE AREAS RESPECTIVELY

DISCHARGE AREA

STATION	DATE	Rn (pCi/L)	He anomaly (ppb)
D7-13	87-10-22	1540	30
D8-9	87-10-22	1290	30
D8-8	87-10-22	1830	50
D8-14	87-10-25	2780	NA
D8-13	87-10-25	1560	90
D8-12	87-10-25	1140	50
D8-11	87-10-25	1200	-10
D8-10	87-10-25	1350	160
D8-10	87-10-25	1360	160
D9-14	87-10-25	1130	NA
D9-14	87-10-25	1290	NA
D9-15	87-10-25	860	40
D9-13	87-10-25	1370	100
D9-13	87-10-25	920	100
D9-12	87-10-25	980	NA
D9-11	87-10-25	280	NA
D9-10	87-10-25	1600	NA
D10-10	87-10-26	1990	50
D10-11	87-10-26	880	50
D10-12	87-10-26	1120	NA
D10-13	87-10-26	1030	100
D10-14	87-10-26	1870	40
D10-15	87-10-26	950	30
D11-15	87-10-26	2190	20
D11-14	87-10-26	970	70
D11-13	87-10-26	870	30
D11-12	87-10-26	1200	NA
D11-11	87-10-26	1000	70
D11-16	87-10-26	2680	120
D11-17	87-10-26	1100	20
D12-18	87-10-26	1270	130
D12-17	87-10-26	1540	-130
D12-16	87-10-26	1220	30
D12-15	87-10-26	1080	-130
D12-14	87-10-26	920	80
D12-13	87-10-26	680	NA
D12-12	87-10-26	1250	0
D13-17	87-10-27	1170	-50
D13-16	87-10-27	1800	0
D13-15	87-10-27	1040	40
D13-14	87-10-27	1100	110
D13-13	87-10-27	900	40
D14-14	87-10-27	1150	170
D14-15	87-10-27	770	120
D14-16	87-10-27	1270	70
D14-17	87-10-27	1650	120
D15-17	87-10-27	990	-10
D15-16	87-10-27	770	30
D15-15	87-10-27	1380	50
D16-18	87-10-27	1160	NA
D16-16	87-10-27	1230	20
D16-17	87-10-27	1500	-30

RECHARGE AREA

STATION	DATE	Rn (pCi/L)	He anomaly (ppb)
12-13-2	87-11-07	370	NA
12-14-2	87-11-07	1380	20
12-1-1	87-10-19	1230	NA
12-1-2	87-10-19	2560	NA
12-1-3	87-10-19	1510	NA
12-15-3	87-11-07	1500	-60
12-15-2	87-11-07	1170	110
12-15-1	87-11-07	1040	50
12-16-1	87-11-07	1230	-10
12-16-2	87-11-07	1710	30
12-16-3	87-11-07	1730	-20
2-2	87-10-03	220	70
2-3	87-10-03	1250	50
2-3	87-10-02	3000	50
2-4	87-10-02	580	-90
2-4	87-10-03	950	-90
2-5	87-10-03	1390	-90
2-5	87-10-06	930	-90
2-6	87-10-07	820	50
2-6	87-10-13	1320	50
2-7	87-10-07	500	-20
2-7	87-10-13	340	-20
2-8	87-10-13	3840	130
2-8	87-10-07	5130	130
2-9	87-10-07	1310	-30
2-9	87-10-13	1360	-30
2-11	87-10-13	1510	-40
2-11	87-10-07	940	-40
2-12	87-10-13	1960	50
2-12	87-10-12	2500	50
2-13	87-10-09	1700	50
2-11	87-10-12	980	-40
2-15	87-10-02	780	-40
2-15	87-10-03	830	-40
2-16	87-10-03	1820	60
2-16	87-10-02	2010	60
2-16	87-10-06	1710	60
2-8-7	87-10-08	2440	NA
2-8-6	87-10-08	3550	NA
2-8-5	87-10-08	5280	NA
2-8	87-10-08	9620	NA
2-8-3	87-10-08	4530	NA
2-8-2	87-10-08	1260	NA
2-8-1	87-10-08	2850	NA
2-8-0	87-10-08	400	NA
23-1-1	87-10-08	2700	NA
23-1-2	87-10-08	1490	NA
3-1	87-10-15	1350	150
3-2	87-10-15	1080	40
3-3	87-10-15	1680	10
3-4	87-10-15	1470	-60
3-2	87-10-15	1410	40

continued...

TABLE 1 (continued)

DISCHARGE AREA

STATION	DATE	Rn (pCi/L)	He anomaly (ppb)
D7-13	87-10-22	1540	30
D8-9	87-10-22	1290	30
D8-8	87-10-22	1830	50
D8-14	87-10-25	2780	NA
D8-13	87-10-25	1560	90
D8-12	87-10-25	1140	50
D8-11	87-10-25	1200	-10
D8-10	87-10-25	1350	160
D8-10	87-10-25	1360	160
D9-14	87-10-25	1130	NA
D9-14	87-10-25	1290	NA
D9-15	87-10-25	860	40
D9-13	87-10-25	1370	100
D9-13	87-10-25	920	100
D9-12	87-10-25	980	NA
D9-11	87-10-25	280	NA
D9-10	87-10-25	1600	NA
D10-10	87-10-26	1990	50
D10-11	87-10-26	880	50
D10-12	87-10-26	1120	NA
D10-13	87-10-26	1030	100
D10-14	87-10-26	1870	40
D10-15	87-10-26	950	30
D11-15	87-10-26	2190	20
D11-14	87-10-26	970	70
D11-13	87-10-26	870	30
D11-12	87-10-26	1200	NA
D11-11	87-10-26	1000	70
D11-16	87-10-26	2680	120
D11-17	87-10-26	1100	20
D12-18	87-10-26	1270	130
D12-17	87-10-26	1540	-130
D12-16	87-10-26	1220	30
D12-15	87-10-26	1080	-130
D12-14	87-10-26	920	80
D12-13	87-10-26	680	NA
D12-12	87-10-26	1250	0
D13-17	87-10-27	1170	-50
D13-16	87-10-27	1800	0
D13-15	87-10-27	1040	40
D13-14	87-10-27	1100	110
D13-13	87-10-27	900	40
D14-14	87-10-27	1150	170
D14-15	87-10-27	770	120
D14-16	87-10-27	1270	70
D14-17	87-10-27	1650	120
D15-17	87-10-27	990	-10
D15-16	87-10-27	770	30
D15-15	87-10-27	1380	50
D16-18	87-10-27	1160	NA
D16-16	87-10-27	1230	20
D16-17	87-10-27	1500	-30

RECHARGE AREA

STATION	DATE	Rn (pCi/L)	He anomaly (ppb)
12-13-2	87-11-07	370	NA
12-14-2	87-11-07	1380	20
12-1-1	87-10-19	1230	NA
12-1-2	87-10-19	2560	NA
12-1-3	87-10-19	1510	NA
12-15-3	87-11-07	1500	-60
12-15-2	87-11-07	1170	110
12-15-1	87-11-07	1040	50
12-16-1	87-11-07	1230	-10
12-16-2	87-11-07	1710	30
12-16-3	87-11-07	1730	-20
2-2	87-10-03	220	70
2-3	87-10-03	1250	50
2-3	87-10-02	3000	50
2-4	87-10-02	580	-90
2-4	87-10-03	950	-90
2-5	87-10-03	1390	-90
2-5	87-10-06	930	-90
2-6	87-10-07	820	50
2-6	87-10-13	1320	50
2-7	87-10-07	500	-20
2-7	87-10-13	340	-20
2-8	87-10-13	3840	130
2-8	87-10-07	5130	130
2-9	87-10-07	1310	-30
2-9	87-10-13	1360	-30
2-11	87-10-13	1510	-40
2-11	87-10-07	940	-40
2-12	87-10-13	1960	50
2-12	87-10-12	2500	50
2-13	87-10-09	1700	50
2-11	87-10-12	980	-40
2-15	87-10-02	780	-40
2-15	87-10-03	830	-40
2-16	87-10-03	1820	60
2-16	87-10-02	2010	60
2-16	87-10-06	1710	60
2-8-7	87-10-08	2440	NA
2-8-6	87-10-08	3550	NA
2-8-5	87-10-08	5280	NA
2-8	87-10-08	9620	NA
2-8-3	87-10-08	4530	NA
2-8-2	87-10-08	1260	NA
2-8-1	87-10-08	2850	NA
2-8-0	87-10-08	400	NA
23-1-1	87-10-08	2700	NA
23-1-2	87-10-08	1490	NA
3-1	87-10-15	1350	150
3-2	87-10-15	1080	40
3-3	87-10-15	1680	10
3-4	87-10-15	1470	-60
3-2	87-10-15	1410	40

continued...

TABLE 1 (continued)

DISCHARGE AREA

STATION	DATE	Rn (pCi/L)	He anomaly (ppb)
D17-18	87-10-27	940	NA
ND1-1	87-10-31	1640	40
ND1-2	87-10-31	2590	100
ND2-1	87-10-31	1400	-20
ND2-2	87-10-31	1190	100
ND2-3	87-10-31	730	100
ND1-3	87-10-31	3440	-20
ND1-4	87-10-31	1380	150
ND1-5	87-10-31	1230	-130
ND2-4	87-10-31	870	0
ND2-5	87-10-31	770	40
ND1-6	87-10-31	880	-10
ND2-6	87-10-31	960	40
ND1-7	87-10-31	1090	140
ND2-9	87-11-02	1200	NA
NWD1-1	87-11-02	4310	120
NWD2-1	87-11-02	2120	110
NWD3-1	87-11-02	2120	100
NWD3-2	87-11-02	1840	-40
NWD2-2	87-11-02	1480	-10
NWD1-2	87-11-02	1790	-40
NWD1-3	87-11-02	1990	-10
NWD2-3	87-11-02	1330	NA
NWD2-4	87-11-02	1120	20
NWD1-4	87-11-02	1420	90
NWD0-4	87-11-02	1640	-50
NWD0-3	87-11-02	1710	80

RECHARGE AREA

STATION	DATE	Rn (pCi/L)	He anomaly (ppb)
3-3	87-10-15	1820	10
3-4	87-10-15	2400	-60
3-5	87-10-15	1340	-20
3-5	87-10-15	1040	-20
3-6	87-10-15	NA	-50
3-7	87-10-15	740	50
3-8	87-10-15	850	50
3-9	87-10-15	2340	20
3-10	87-10-15	1630	-20
3-11	87-10-15	1100	40
3-12	87-10-15	1750	250
3-12	87-10-16	5120	250
3-12	87-10-17	4190	250
3-13	87-10-16	3720	100
3-13	87-10-16	4450	100
3-14	87-10-16	3360	40
3-15	87-10-16	3200	NA
3-15	87-10-16	2930	NA
3-16	87-10-17	4250	410
3-16	87-10-17	4040	410
3-17	87-10-16	3790	-50
3-17	87-10-17	4050	-50
3-17	87-10-17	3460	-50
3-18	87-10-16	1410	60
3-18	87-10-16	1310	60
3-19	87-10-16	1350	0
3-19	87-10-16	1130	0
3-19	87-10-17	1280	0
3-19	87-10-17	1400	0
3-20	87-10-17	3930	10
3-20	87-10-17	3850	10
3-21	87-10-17	2090	30
34-15-1	87-10-28	1500	50
34-15-3	87-10-28	2390	-30
4-1	87-10-19	1570	40
4-2	87-10-19	2430	20
4-3	87-10-19	1680	0
4-4	87-10-19	620	-60
4-5	87-10-19	1700	60
4-6	87-10-19	1680	NA
4-7	87-10-19	2640	-20
4-8	87-10-19	2730	NA
4PS-1	87-10-25	660	0
4PS-2	87-10-25	1670	-60
4PS-3	87-10-25	1040	0
4PS-4	87-10-25	1050	-20
EW-1	87-10-18	1630	-10
EW-1	87-10-18	2090	-10
EW-3	87-10-18	1500	-60
EW-3	87-10-18	1950	-60
EW-4	87-10-18	1700	30
EW-4	87-10-18	1330	30

continued...

TABLE 1 (concluded)

DISCHARGE AREA

STATION	DATE	Rn (pCi/L)	He anomaly (ppb)

RECHARGE AREA

STATION	DATE	Rn (pCi/L)	He anomaly (ppb)
EW-5	87-10-18	1010	40
EW-5	87-10-18	970	40
EW-6	87-10-18	3130	40
EW-6	87-10-18	4220	40
EW-7	87-10-18	3240	-20
EW-7	87-10-18	4570	-20
EW-8	87-10-18	4690	NA
EW-8	87-10-18	6040	NA
EW-9	87-10-18	490	-70
EW-9	87-10-18	700	-70
2-18	87-10-02	510	NA
2-18	87-10-03	550	NA
2-18	87-10-06	560	NA
2-18	87-10-07	510	NA
2-18	87-10-09	500	NA
2-18	87-10-13	610	NA
2-18	87-10-15	570	NA
2-18	87-11-03	580	NA
2-18	87-11-11	580	NA
2-18	87-11-12	580	NA

TABLE 2

CONCENTRATION OF RADON IN GROUNDWATERS SAMPLED FROM PIEZOMETER ZONES IN EAST SWAMP AREA

Piezometer	Level	Date	^{222}Rn (pCi/L)	Comments
100	I	2-12-87	418	
	II	2-12-87	1060	
101	I	2-12-87	-	dry
	II	2-12-87	933	
102	I	2-12-87	-	near dry
103	I	3-12-87	93	
	II	3-12-87	30	
	III	3-12-87	113	
104	I	3-12-87	48	
	II	3-12-87	600	
105	I	4-12-87	-	sample lost
	II	4-12-87	1582	
106				not sampled
107	I	3-12-87	625	
	II	3-12-87	2495	
109	I	3-12-87	50	near dry
110	I	3-12-87	-	dry
111	I	4-12-87	-	not sampled
	II	4-12-87	-	not sampled
112	I	4-12-87	-	dry
	II	4-12-87	72	
114	I	2-12-87	105	
	II	2-12-87	41	
115	I	2-12-87	-	dirty sample
	II	2-12-87	766	
	III	2-12-87	1325	
	IV	2-12-87	1500	
116	I	2-12-87	-	near dry
117	I	4-12-87	200	
	II	4-12-87	27	
	III	4-12-87	-	frozen
118	I	3-12-87	93	
	II	3-12-87	483	

TABLE 3

SUMMARY OF RADON CONCENTRATIONS IN SOIL GASES AT GRID SITES

Grid Coordinate SSW	Grid Coordinate ESE	Rn (pCi/L)	Grid Coordinate SSW	Grid Coordinate ESE	Rn (pCi/L)	Grid Coordinate SSW	Grid Coordinate ESE	Rn (pCi/L)
1.00	1.00	800	3.00	9.00	660	7.00	5.00	560
1.00	2.00	830	3.00	10.00	1440	7.00	6.00	570
1.00	3.00	1180	3.00	11.00	1240	7.00	7.00	640
1.00	4.00	460	3.00	11.50	2180	7.00	8.00	510
1.00	5.00	700	3.00	12.00	3660	7.00	9.00	960
1.00	6.00	850	3.00	12.00	3750	7.00	10.00	1070
1.00	7.00	810	3.25	7.75	770	7.00	11.00	1450
1.00	7.50	770	3.25	8.00	1060	7.00	12.00	2060
1.00	8.00	1320	3.25	8.25	800	8.00	1.00	260
1.00	8.50	1080	3.50	8.00	1070	8.00	2.00	790
1.00	9.00	1100	3.50	9.50	670	8.00	3.00	710
1.00	10.00	1090	4.00	1.00	710	8.00	4.00	840
1.00	11.00	1380	4.00	2.00	810	8.00	5.00	440
1.00	12.00	4390	4.00	3.00	780	8.00	6.00	700
1.50	7.00	860	4.00	4.00	740	8.00	7.00	610
1.50	7.50	960	4.00	5.00	470	8.00	8.00	660
1.50	8.00	990	4.00	6.00	630	8.00	9.00	1980
1.50	8.50	880	4.00	7.00	710	8.00	10.00	1000
2.00	1.00	690	4.00	8.00	960	8.00	11.00	1070
2.00	2.00	880	4.00	9.00	1080	8.00	11.80	940
2.00	3.00	1110	4.00	10.00	1220	9.00	1.00	460
2.00	4.00	750	4.00	11.00	1170	9.00	2.00	870
2.00	5.00	650	4.00	12.00	4080	9.00	3.00	660
2.00	6.00	520	5.00	1.00	450	9.00	4.00	860
2.00	7.00	750	5.00	2.00	920	9.00	5.00	480
2.00	7.50	920	5.00	3.00	890	9.00	6.00	660
2.00	8.00	5810	5.00	4.00	630	9.00	7.00	1070
2.00	8.00	6160	5.00	5.00	600	9.00	8.00	700
2.00	8.00	6380	5.00	6.00	500	9.00	9.00	1330
2.00	8.50	650	5.00	7.00	540	9.00	10.00	910
2.00	9.00	970	5.00	8.00	840	9.00	11.00	1220
2.00	10.00	930	5.00	9.00	1260	10.00	1.00	500
2.00	11.00	1170	5.00	10.00	1370	10.00	2.00	780
2.00	12.00	5400	5.00	11.00	1250	10.00	3.00	720
2.50	7.50	730	5.00	12.00	1910	10.00	4.00	890
2.50	8.00	840	5.50	6.50	710	10.00	5.00	730
2.50	9.00	520	5.50	10.50	750	10.00	6.00	680
2.75	7.75	1090	6.00	1.00	380	10.00	7.00	520
2.75	8.00	1450	6.00	2.00	1000	10.00	8.00	560
2.75	8.25	1050	6.00	3.00	850	10.00	9.00	930
3.00	1.00	600	6.00	4.00	890	10.00	10.00	520
3.00	2.00	780	6.00	5.00	640	10.00	11.00	600
3.00	3.00	880	6.00	6.00	370	11.00	1.00	600
3.00	4.00	600	6.00	7.00	980	11.00	2.00	740
3.00	5.00	750	6.00	8.00	1590	11.00	3.00	810
3.00	6.00	320	6.00	9.00	4820	11.00	4.00	970
3.00	7.00	600	6.00	10.00	1130	11.00	5.00	720
3.00	7.50	680	6.00	11.00	1260	11.00	6.00	530
3.00	7.75	1060	6.00	12.00	3120	11.00	7.00	420
3.00	8.00	2630	6.50	5.50	820	11.00	8.00	770
3.00	8.00	2630	7.00	1.00	600	11.00	9.00	880
3.00	8.25	820	7.00	2.00	690	11.00	10.00	690
3.00	8.50	400	7.00	3.00	620	11.00	11.00	440
3.00	8.75	720	7.00	4.00	830			

TABLE 4

He AND Rn CONCENTRATIONS IN GROUNDWATERS ASSOCIATED WITH FZ2 IN THE URL LEASE AREA BOREHOLES (UPPER) AND 240-m LEVEL BOREHOLES (MIDDLE) AND VERTICAL FRACTURES AT THE 240-m LEVEL (LOWER)

Borehole Zone	Depth (m)	Date Sampled	He (cm^3/L)	^{222}Rn (pCi/L)
M1A-3-1	240-324	21 Apr 86	16.03	
M2A-3-4	270-400	29 May 86	5.67	
M3A-3-6	351-400	07 Jul 88	12.04	945
M4A-4-6	291-406	14 Jul 86	56.31	
M5B-2-6	106-151	12 Oct 88	0.96	6 500
M8-3-7A/17	340-380	09 Jun 86 (He) 23 Oct 88 (Rn)	1.45	10 800
M13-2-3B	226-443	16 Jun 86	11.32	
B34-1-4C	32.5-60	24 Oct 86 (He) 28 Jul 88 (Rn)	5.10	5 700
URL10-6-7a	270-302	09 Jul 86	7.48	
URL11-7-7	183-202	20 Nov 88		25 400
URL12-11-13	458-502	11 Sept 86	29.3	
HC6-17		07 Jun 89	6.01	9 300
HC7-17		07 Jun 89	10.04	5 700
HC8-16		11 Apr 89	7.60	6 200
HC9-17		15 Jun 89	6.41	6 300
HC11-16		11 Apr 89	11.62	14 900
HC12-17		20 Jun 89	11.23	9 000
HC14-17		15 Jun 89	12.49	160
HC15-16		11 Apr 89	11.15	5 200
HC16-16		11 Apr 89	2.47	8 700
HC18-10		29 Jan 88	9.86	
HC18-16		11 Apr 89		28 600
HC19-17		20 Jun 89		10 100
HC23-10		29 Jan 88	3.08	
HC23-17		20 Jun 89		2 800
HC24-17		15 Jun 89		7 000
HC26-16		11 Apr 89		3 000
HC27-10		29 Jan 88	6.26	
HC27-16		11 Apr 89		3 600
HC28-16		11 Apr 89		4 500
HC29-16		11 Apr 89		1 200
HC30-16		11 Apr 89		5 000
HC31-16		11 Apr 89		1 100
HC32-16		11 Apr 89		3 100
JE1-17		15 Jun 89		29 500
PH3-Z4-12		08 Jun 88	11.63	19 700
PH5-Z4-17		15 Jun 89		49 300
209-010-0C1-12		08 Jun 88		29 200
209-0C1(N3)-4A		21 Aug 86	13.05	

TABLE 5

INJECTION PRESSURES AND ESTIMATED BREAKTHROUGH TIMES FOR GAS INJECTION TESTS

Case	Rock Only - Case 1	Rock and Overburden	
		Rock - Case 2	Overburden - Case 3
Input Parameters			
Depth of rock or overburden (m)	40	27	13
Hydraulic conductivity (m/s)	2×10^{-6}	2×10^{-6}	2×10^{-9}
Angle of inclination to horizontal (°)	20°	20°	90°
Fracture spacing (m)	27	27	1
Calculated Parameters			
Path length for gas (m)	117	79	13
Effective fracture width (m)	0.44×10^{-3}	0.44×10^{-3}	0.015×10^{-3}
Capillary pressure (MPa)	0.34×10^{-3}	0.34×10^{-3}	0.01
Threshold pressure (MPa)	0.39	0.39	0.40
Injection Pressure (MPa)	Breakthrough Time* (d)		
0.393	0.21	0.14	0.23
0.403	0.090	0.053	0.22
0.413	0.070	0.040	0.21
0.423	0.060	0.034	0.21
0.433	0.052	0.029	0.20
0.443	0.047	0.026	0.19
0.453	0.043	0.023	0.19
0.463	0.039	0.021	0.18
0.473	0.037	0.020	0.18
0.483	0.034	0.018	0.17
0.493	0.032	0.017	0.17

* Breakthrough times may be up to 100 times greater because of time taken to fill excess porosity in non-uniform cracks. "Best estimates" are 20-30 times greater than shown.

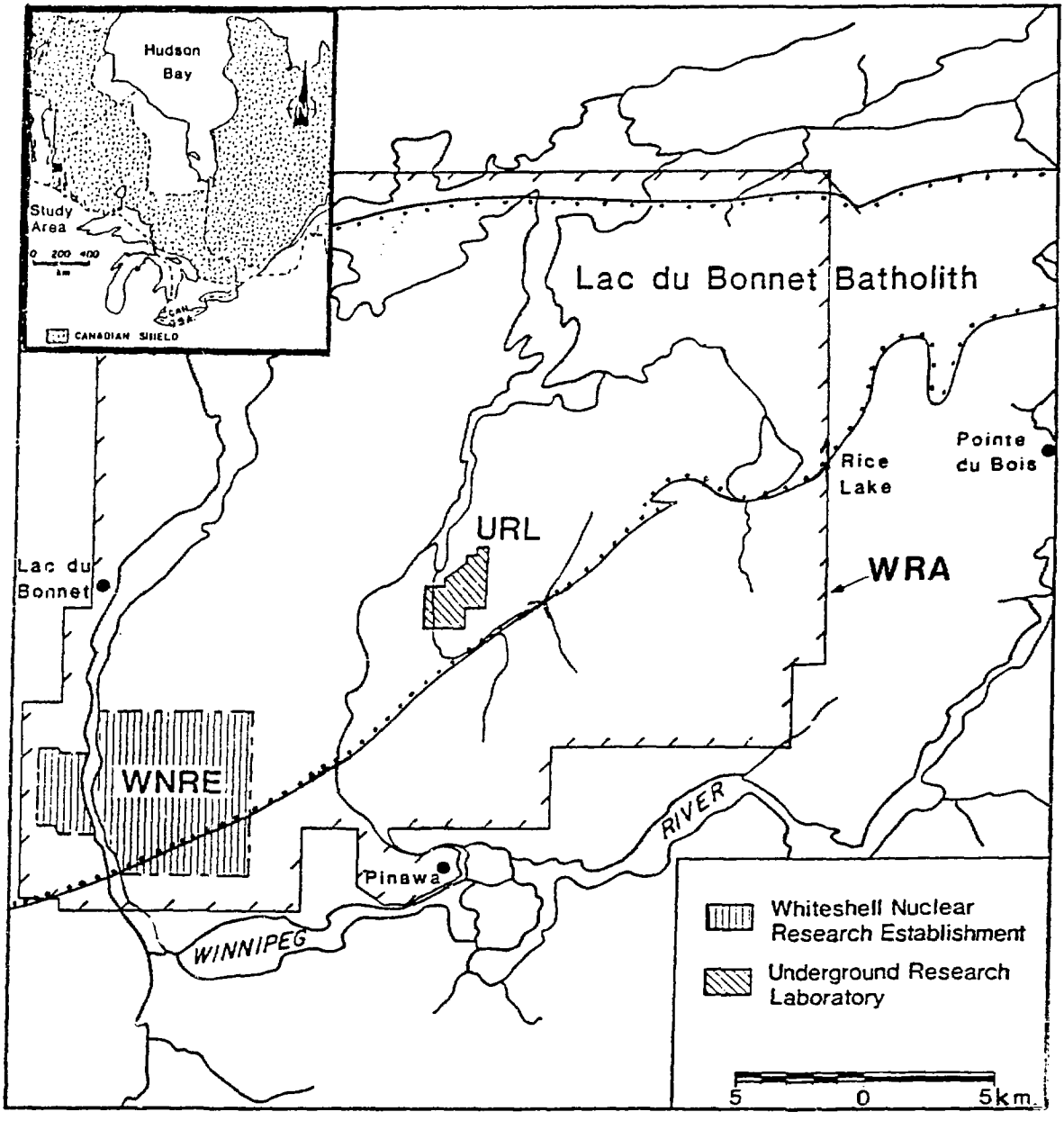

FIGURE 1: Location of the Underground Research Laboratory (URL) with Respect to the Whiteshell Laboratories, the Whiteshell Research Area (WRA) and the Outcrop of the Lac du Bonnet Granite Batholith (dotted boundary). The inset shows the location of this region with respect to the Canadian Shield.

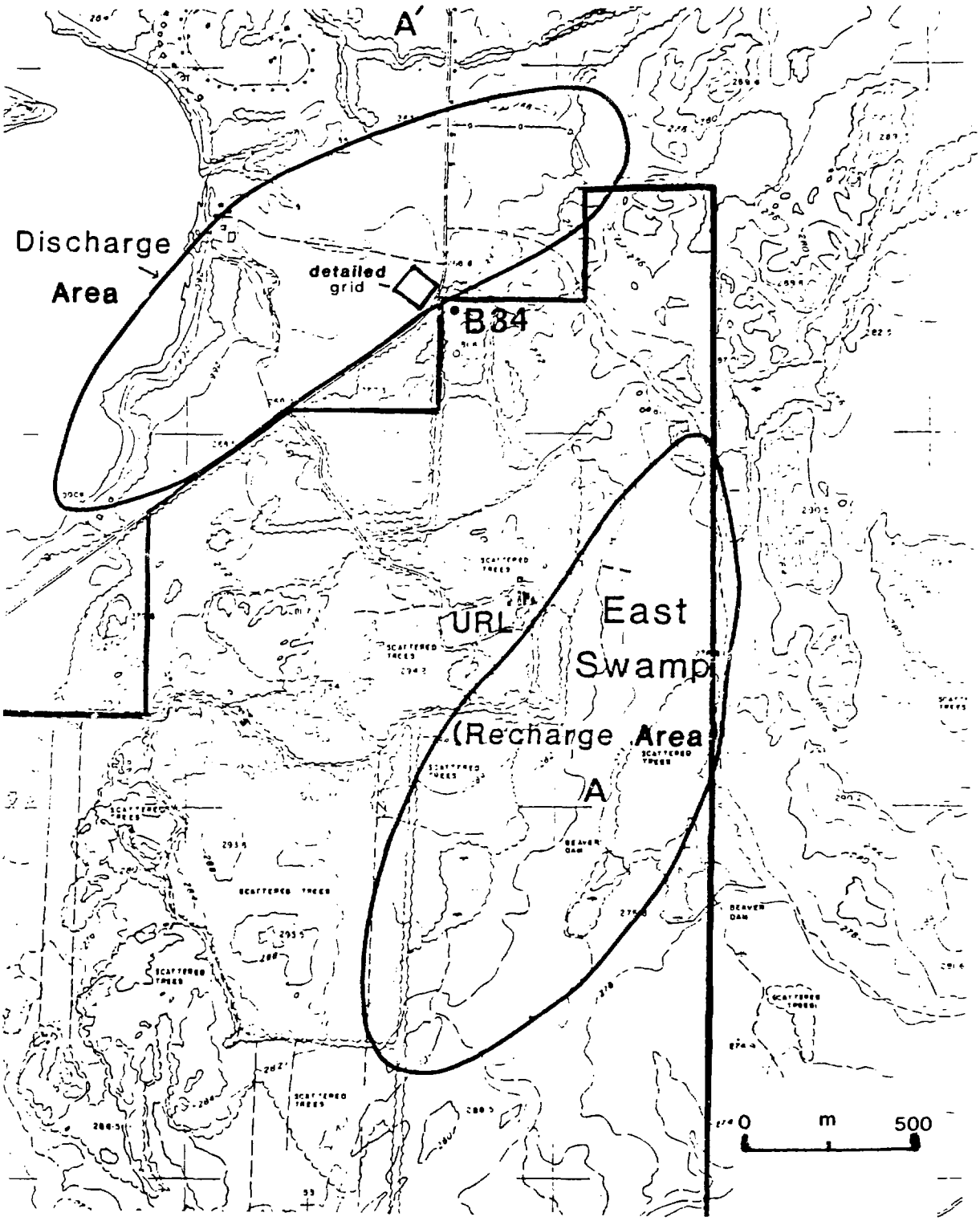

FIGURE 2: Location of the "Recharge" and "Discharge" Zones for Groundwater with Respect to the URL Lease Area (outlined)

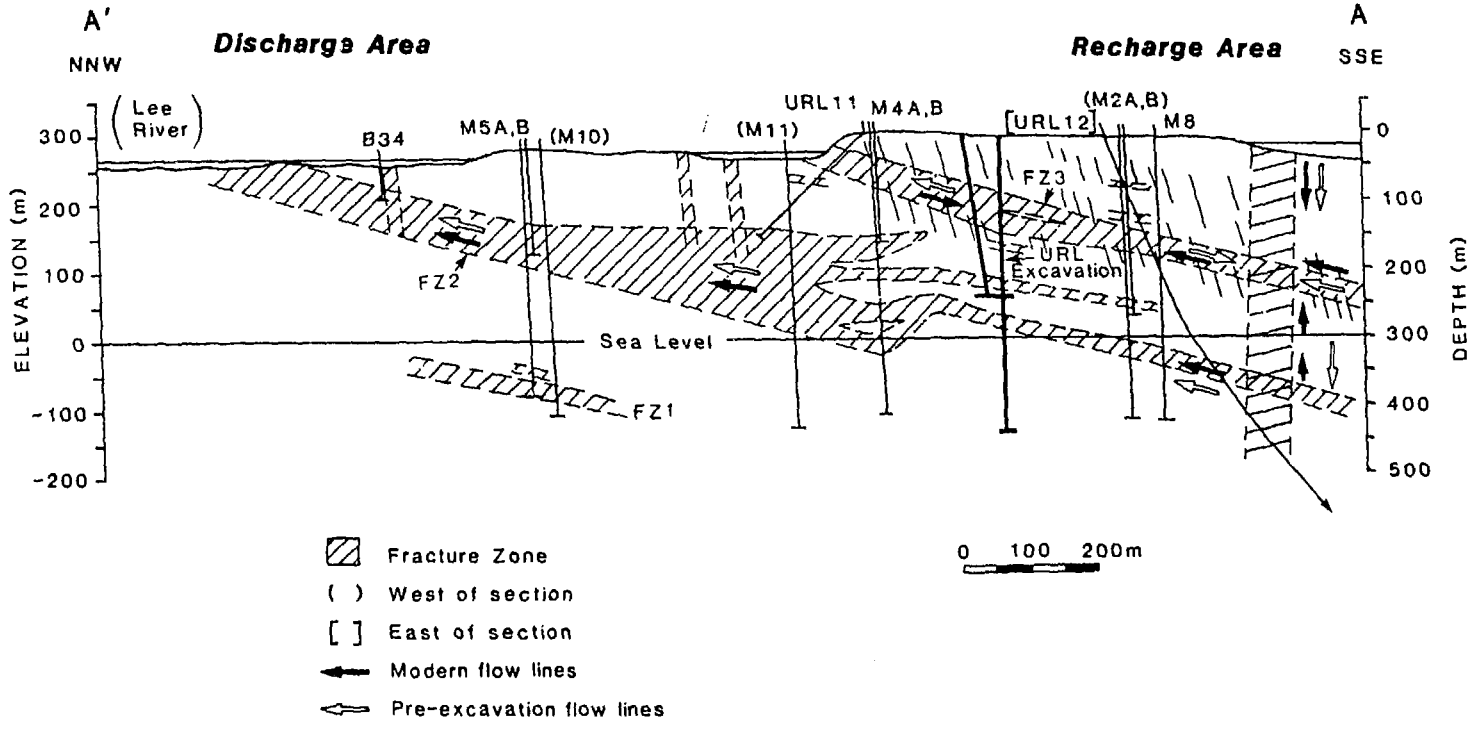

FIGURE 3: Cross Section Through the URL Showing Groundwater Flow Paths in Relation to the Recharge and Discharge Areas. Boreholes (numbered) are shown as steep or vertical lines.

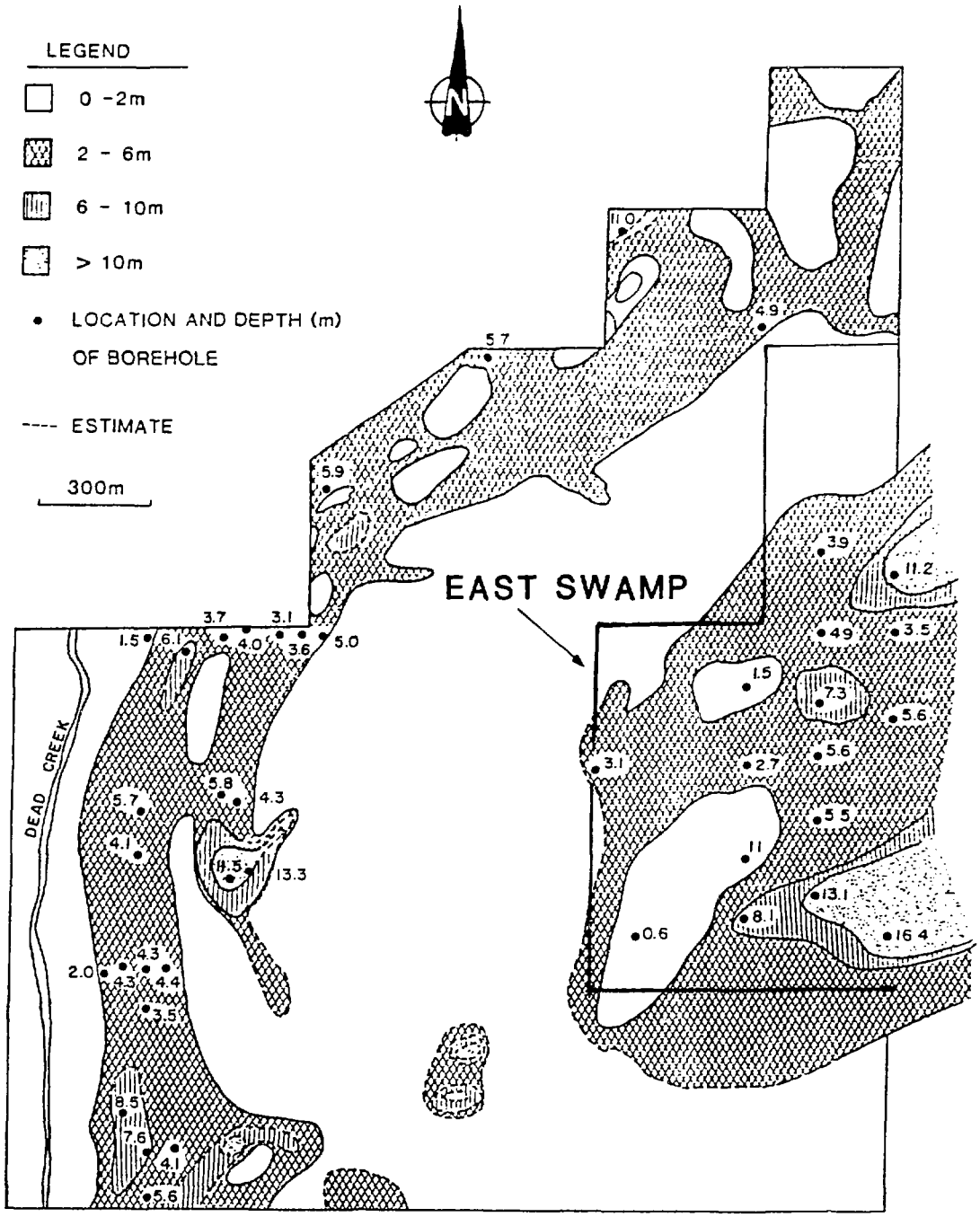

FIGURE 4: Location and Thicknesses of Overburden on the URL Lease Area (from Killey, personal communication, 1987). The large area to the centre right describes the "recharge" area.

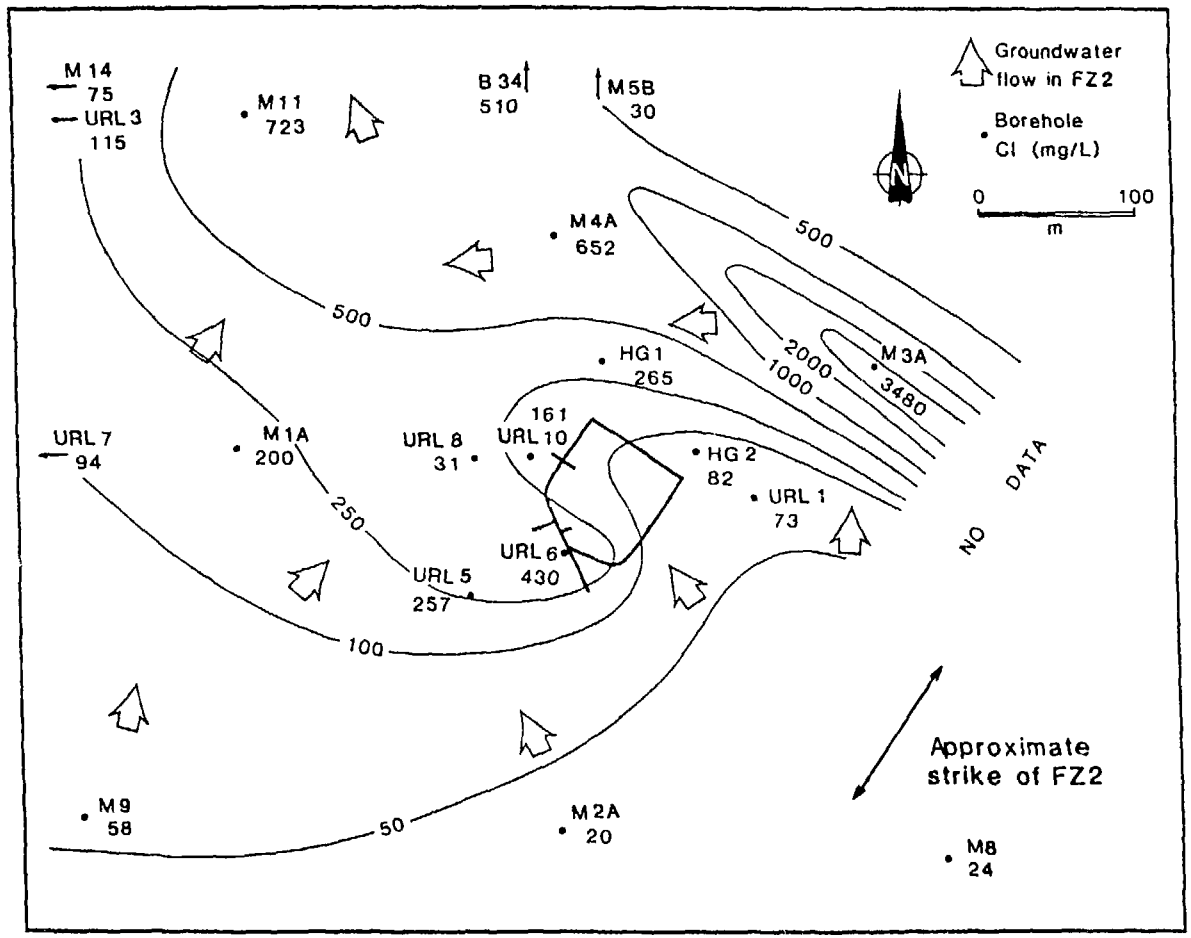

FIGURE 5: Plan of Surface Boreholes that Intersect FZ2 and the Location of the URL 240-m Level, Showing Variation in Cl Concentration of Groundwater and Approximate Groundwater Flow Directions (from Gascoyne et al. 1989)

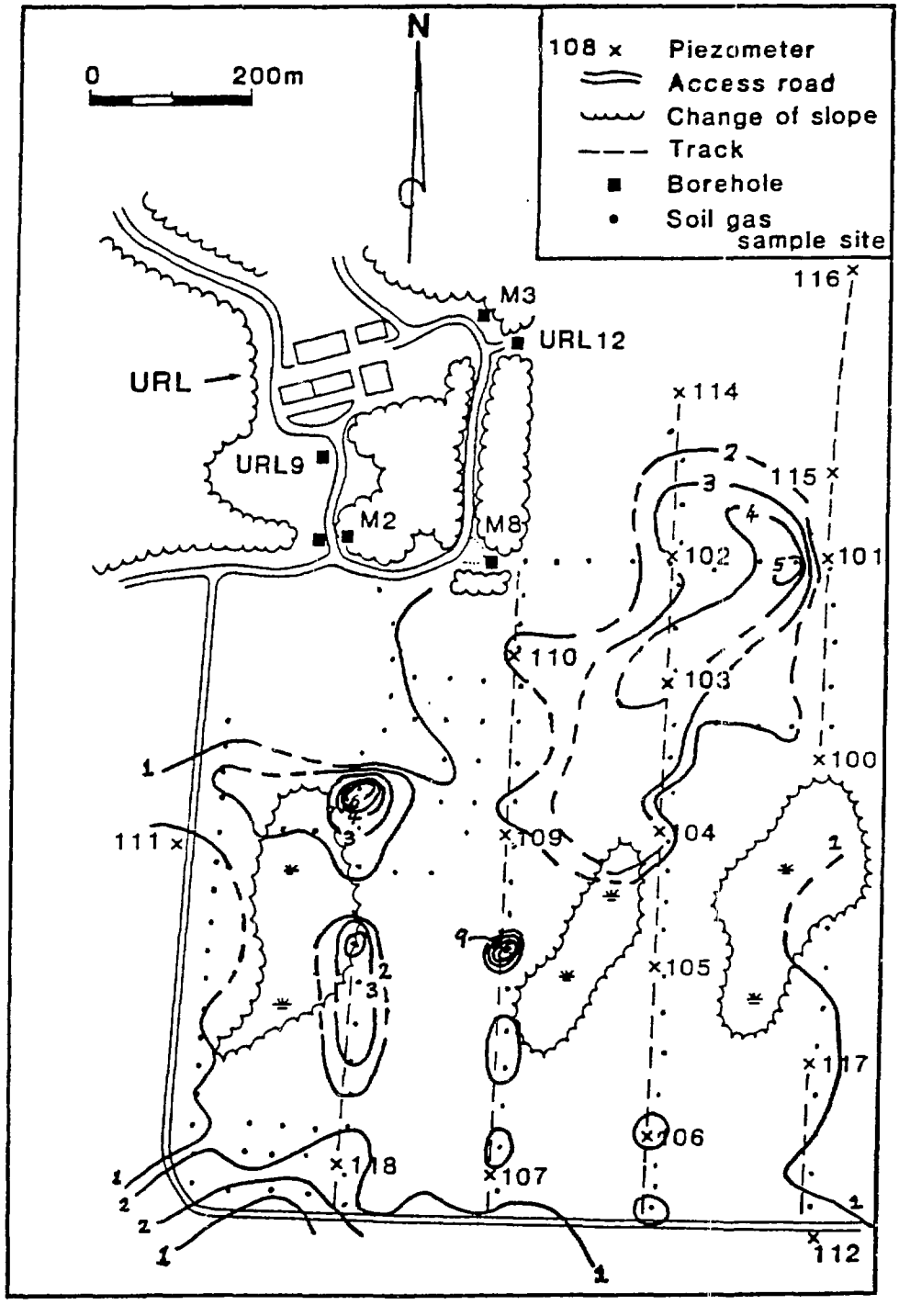

FIGURE 6a: Variations, Expressed as Contours of Rn Content x 10^3 (pCi/L), of Soil Gases Sampled in the Recharge Area

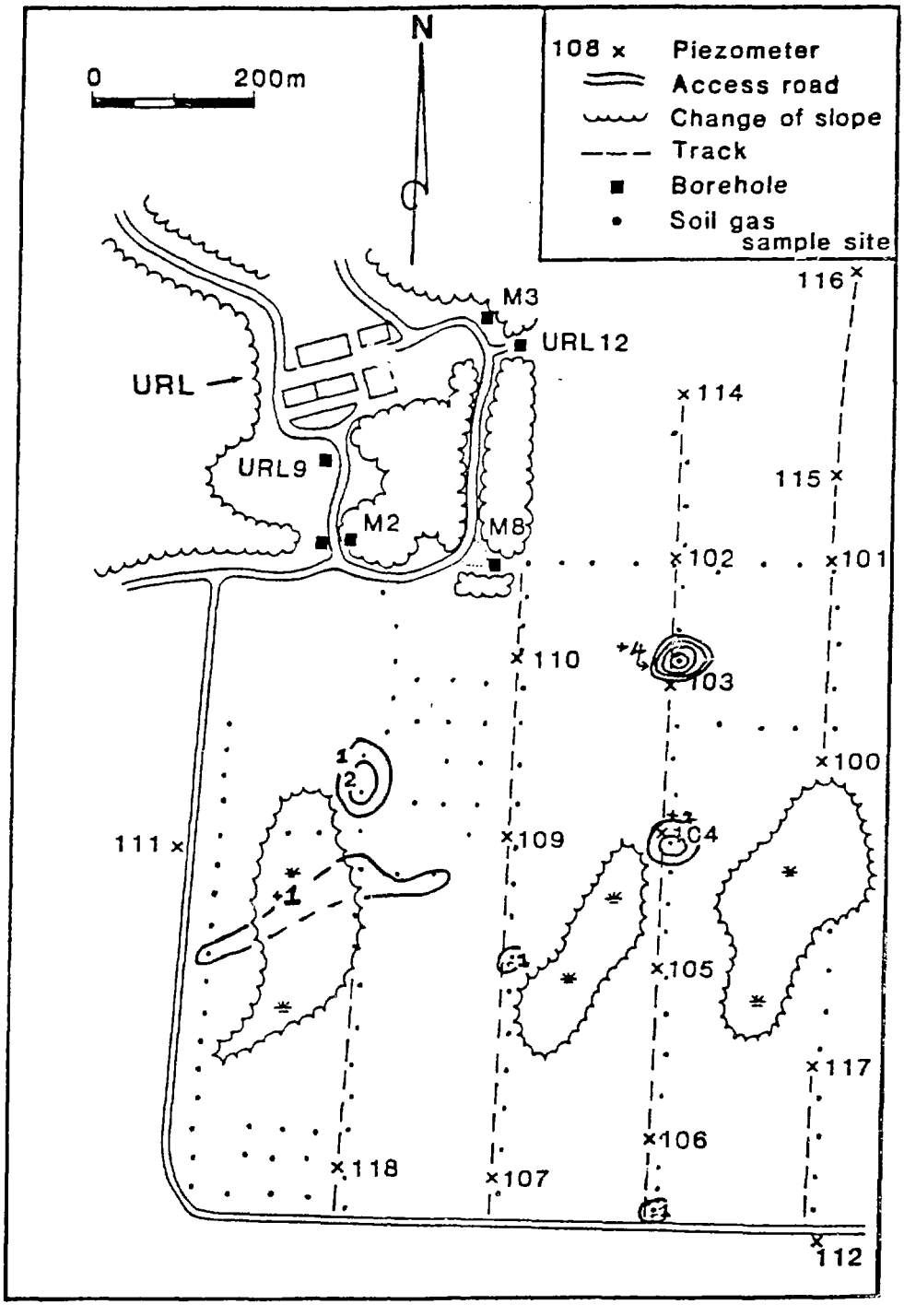

FIGURE 6b: Variations, Expressed as Contours of He Content x 10^2 (as Difference to Air, ppb), of Soil Gases Sampled in the Recharge Area

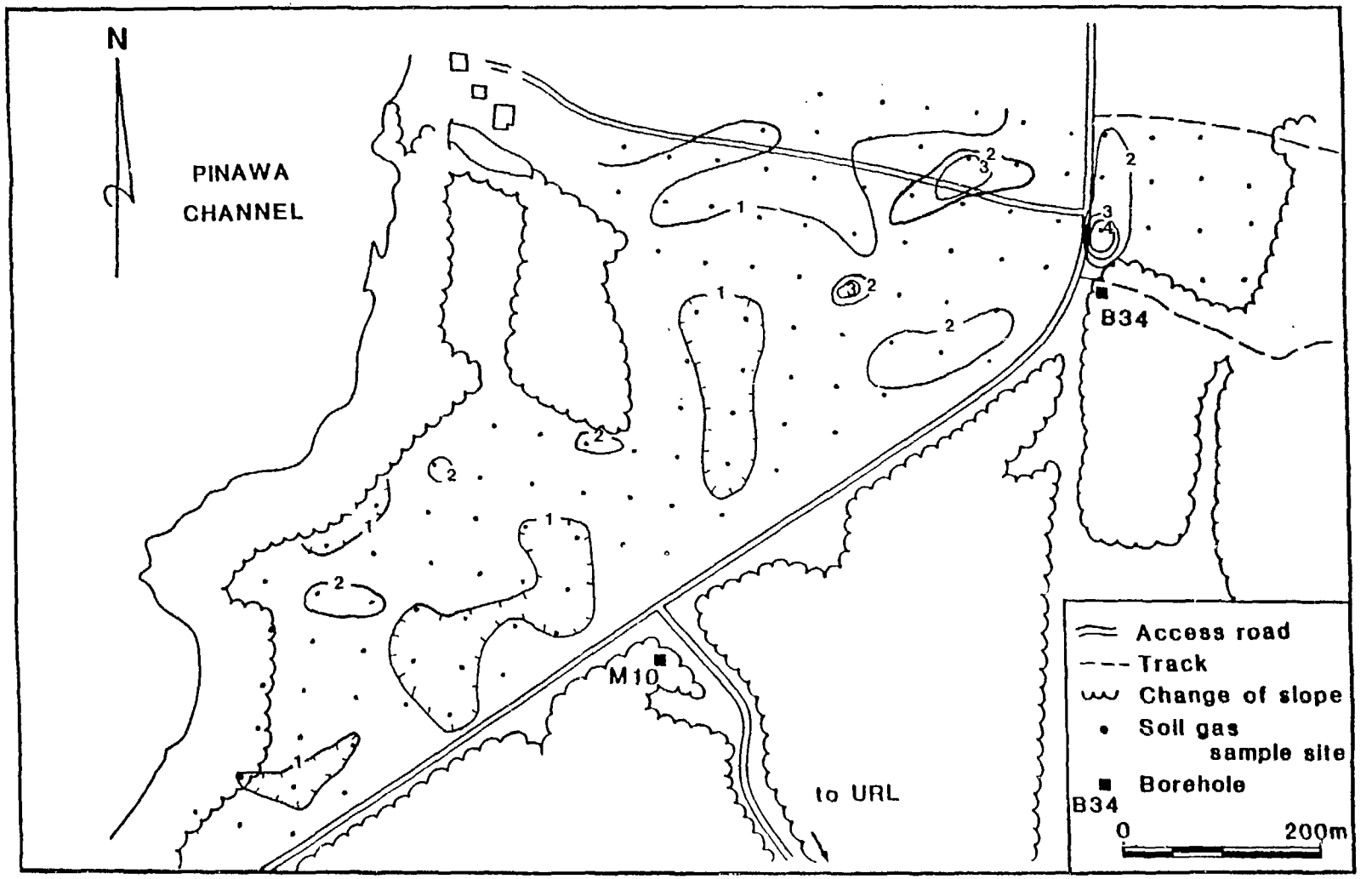

FIGURE 7a: Variations, Expressed as Contours of Rn Content x 10^3 (pCi/L), of Soil Gases Sampled in the Discharge Area

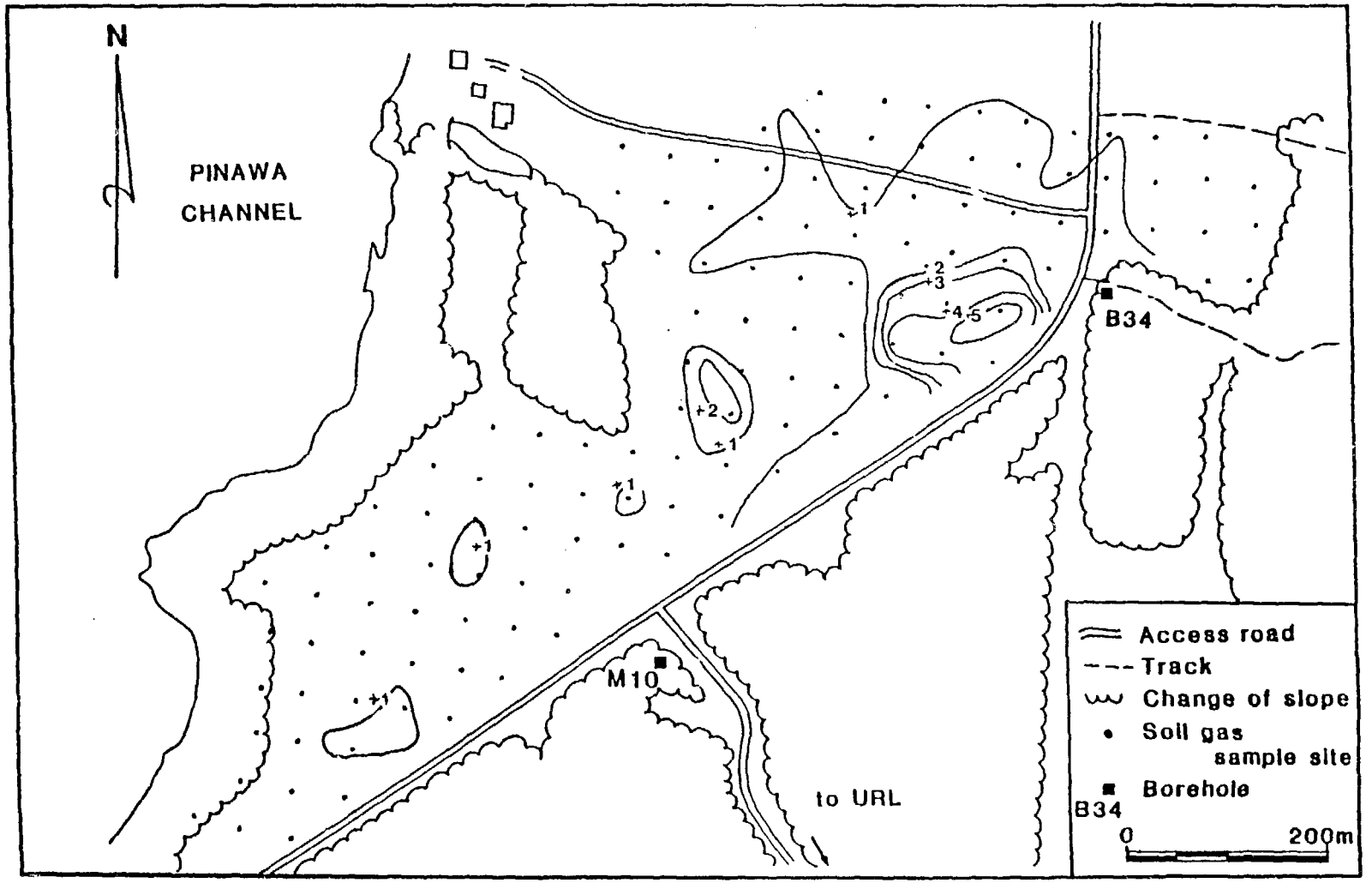

FIGURE 7b: Variations, Expressed as Contours of He Content x 10^2 (As Difference to Air, ppb), of Soil Gases Sampled in the Discharge Area

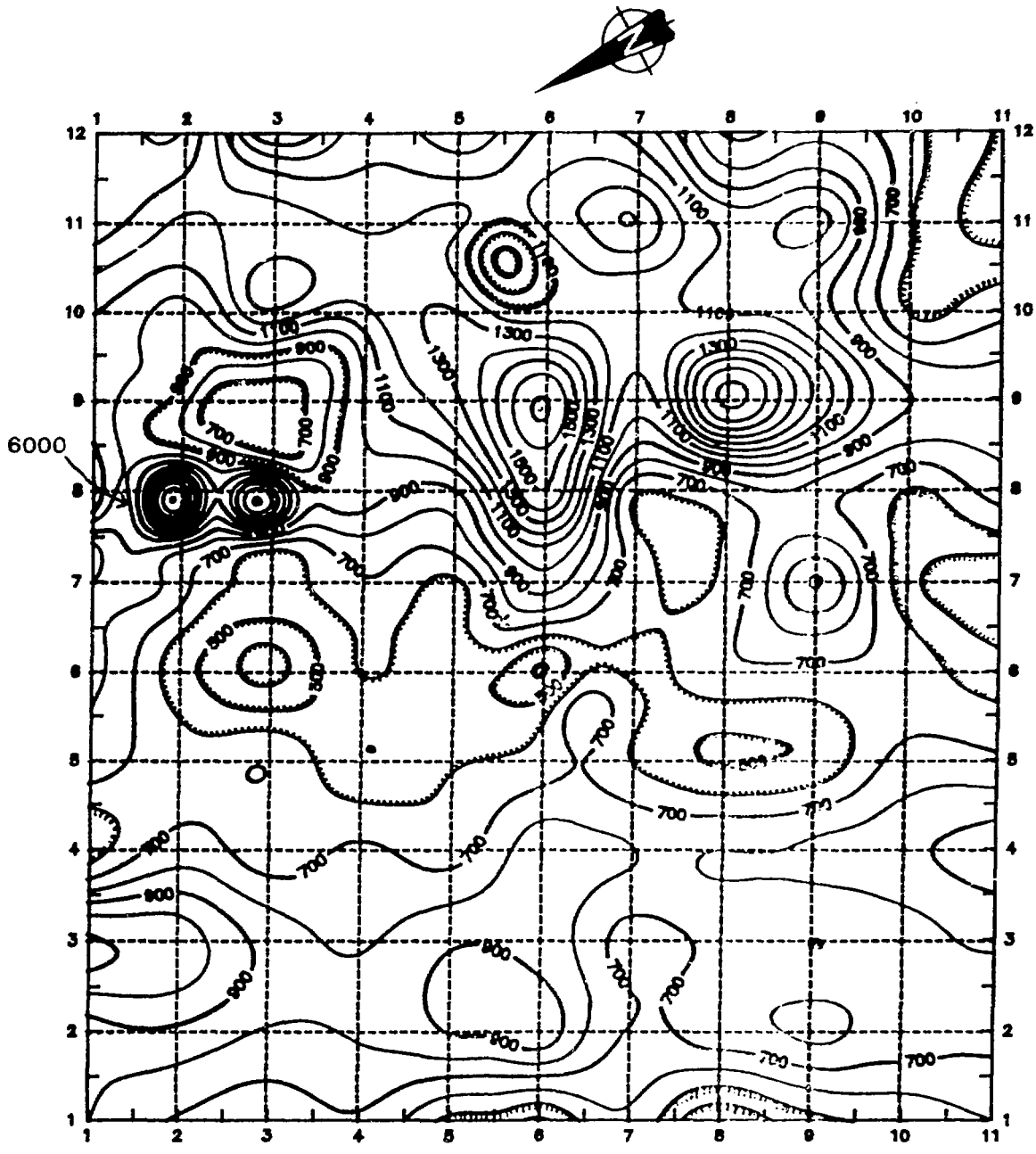

FIGURE 8: Contour Map of Radon Concentrations (pCi/L) in Soil Gas for the Detailed Grid Shown in Figure 2. Each grid segment is 10 m x 10 m.

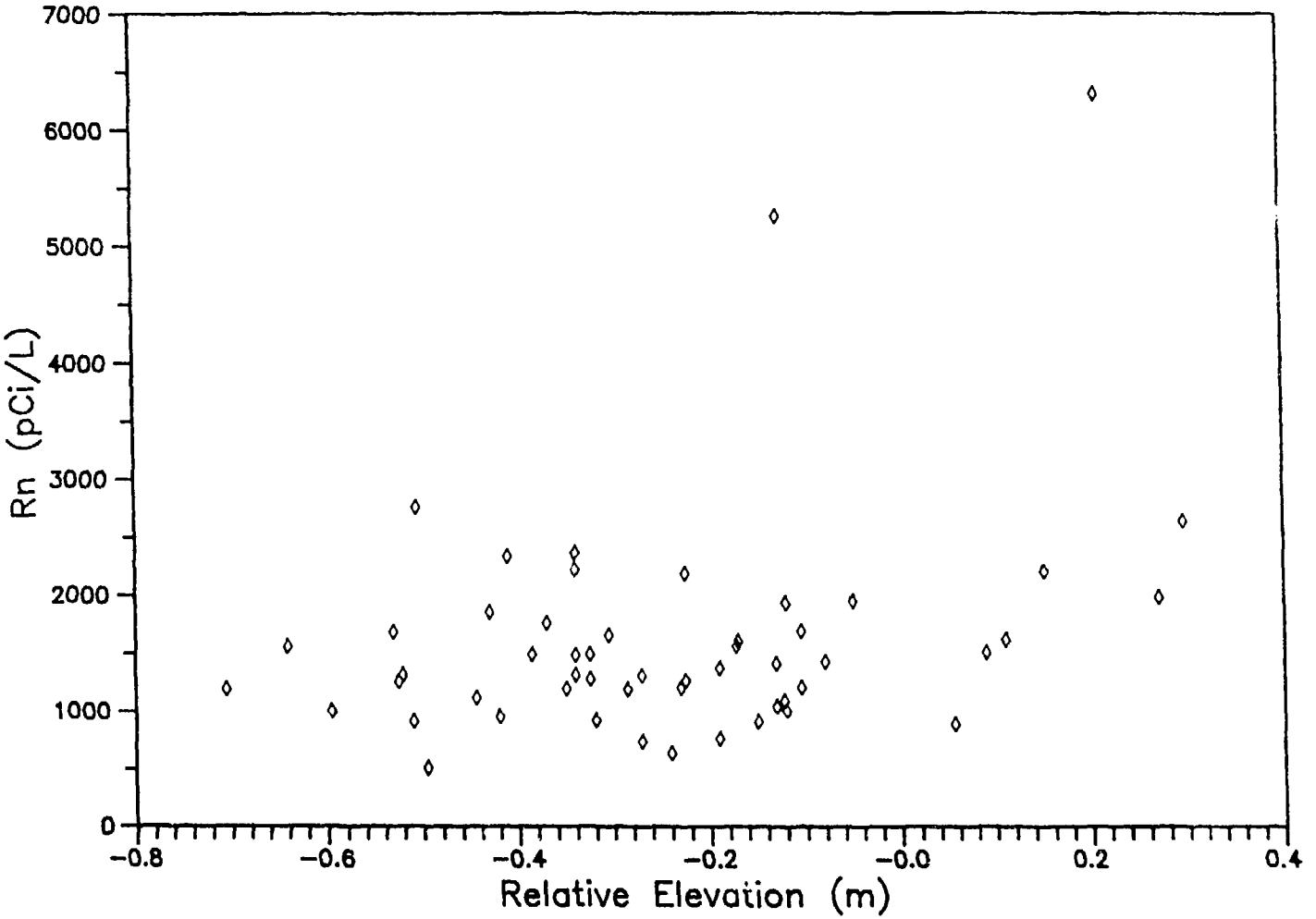

FIGURE 9: Plot of Soil Gas Radon Levels With Respect to Elevation Relative to the Standard Site

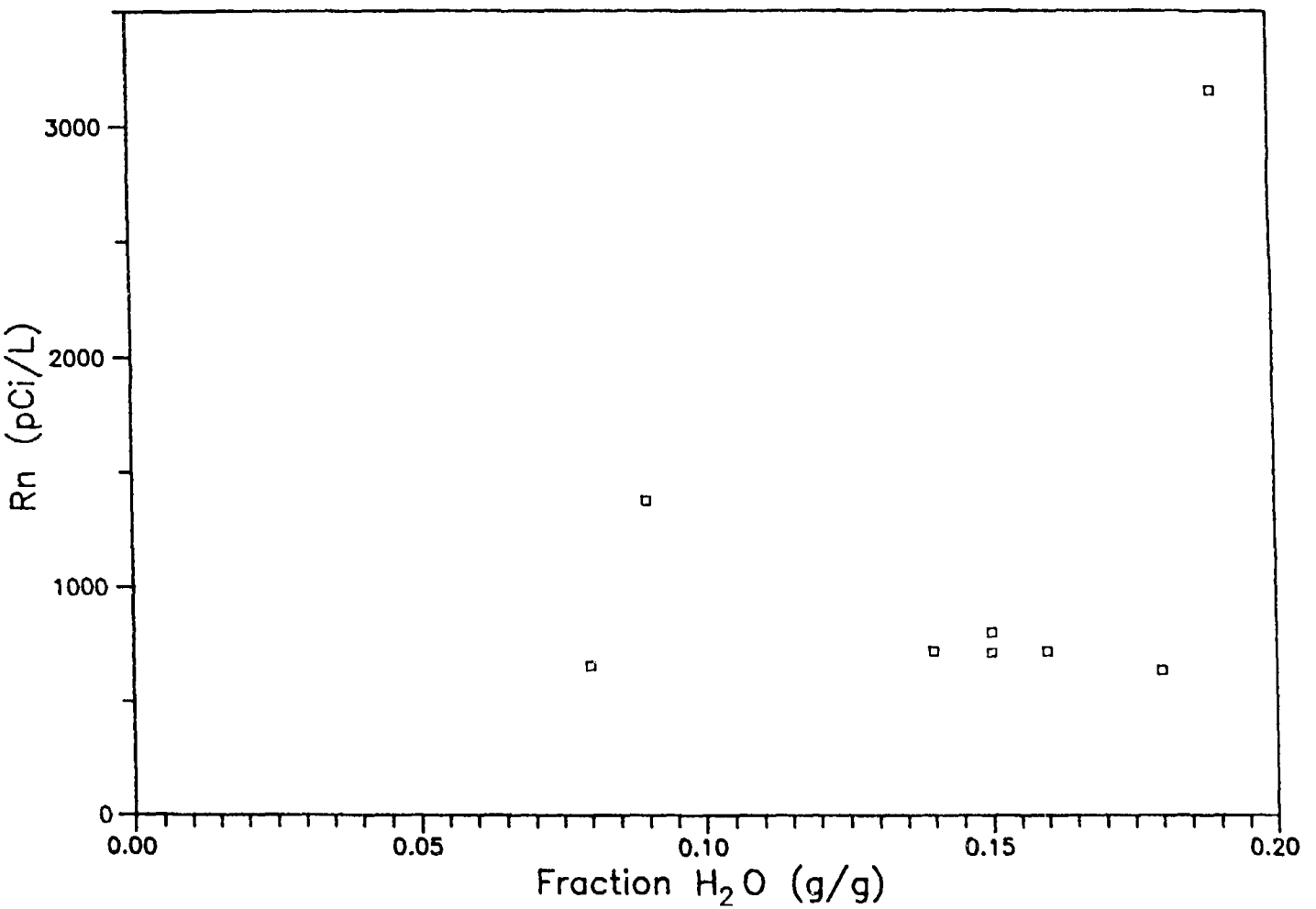

FIGURE 10: Plot of Soil Gas Radon Levels with Respect to Water Content of the Soil

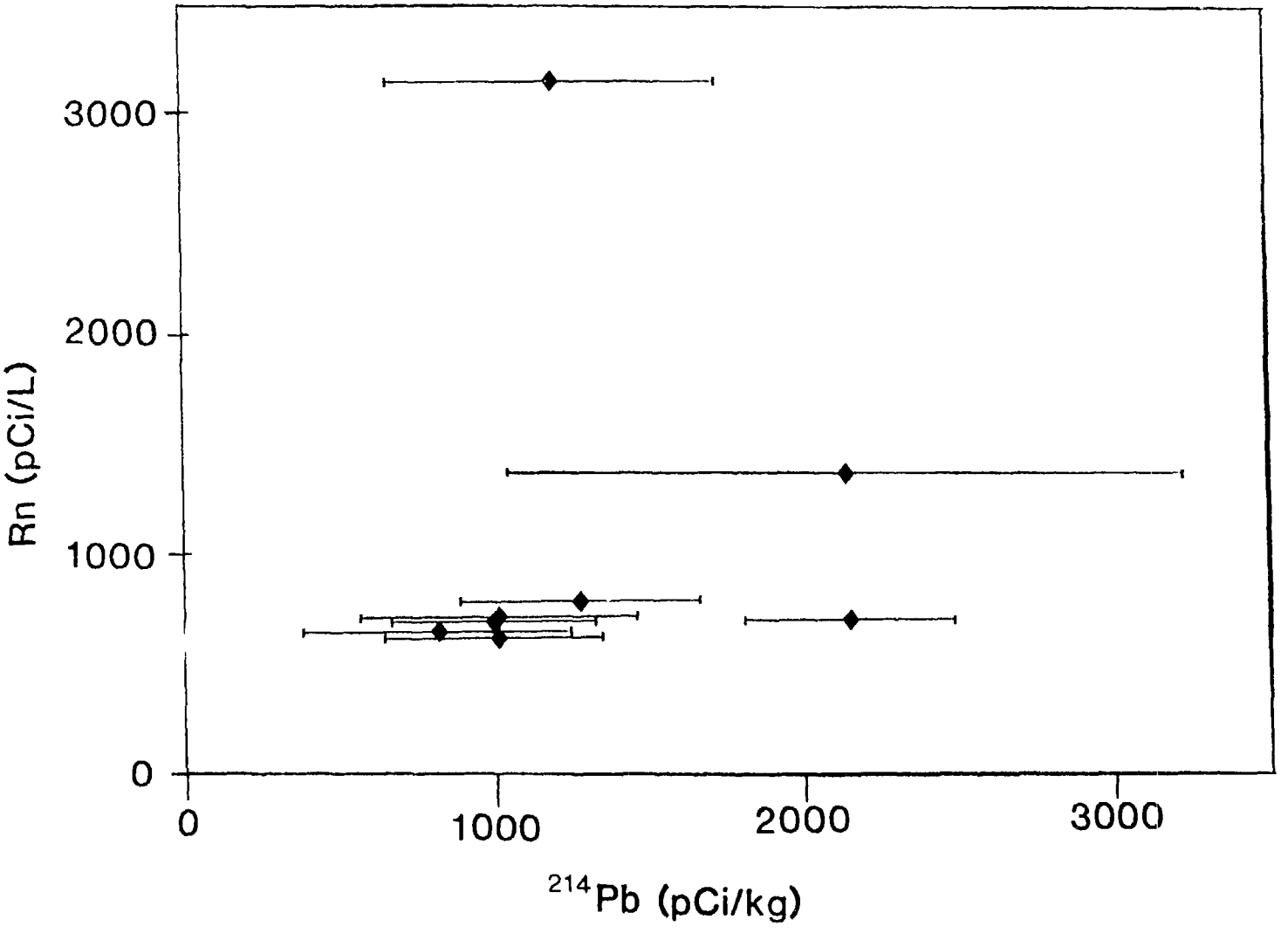

FIGURE 11: Plot of Soil Gas Radon Level with Respect to ^{226}Ra Content of Soils (Measured as ^{214}Pb at Equilibrium). Error bars are $\pm 1\sigma$.

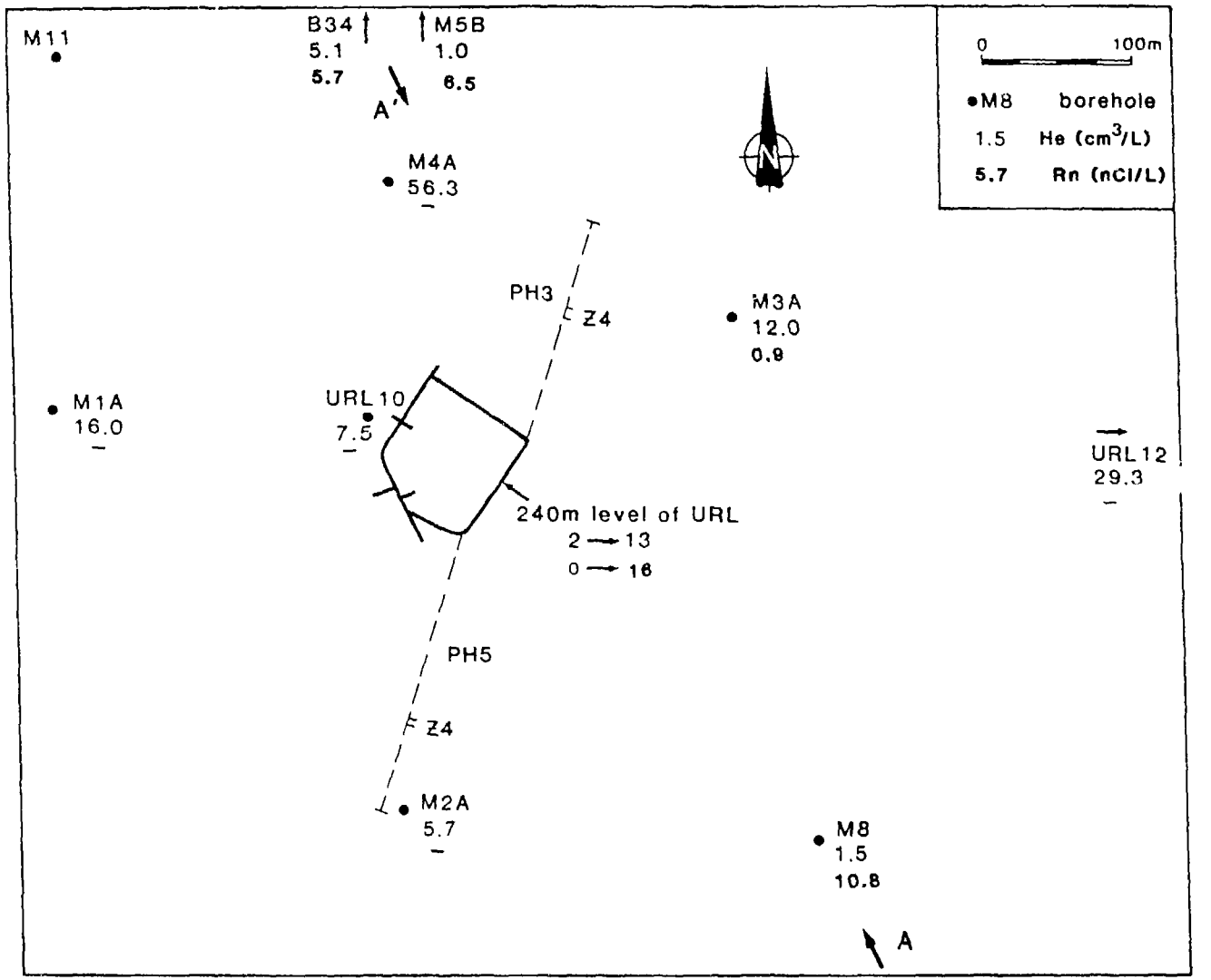

FIGURE 12: Location of Surface Boreholes that Intersect FZ2 in the URL Lease Area Showing Values of He (Upper) and Rn (Lower) Concentrations in Groundwater. Figure 3 is drawn approximately along section A-A'.

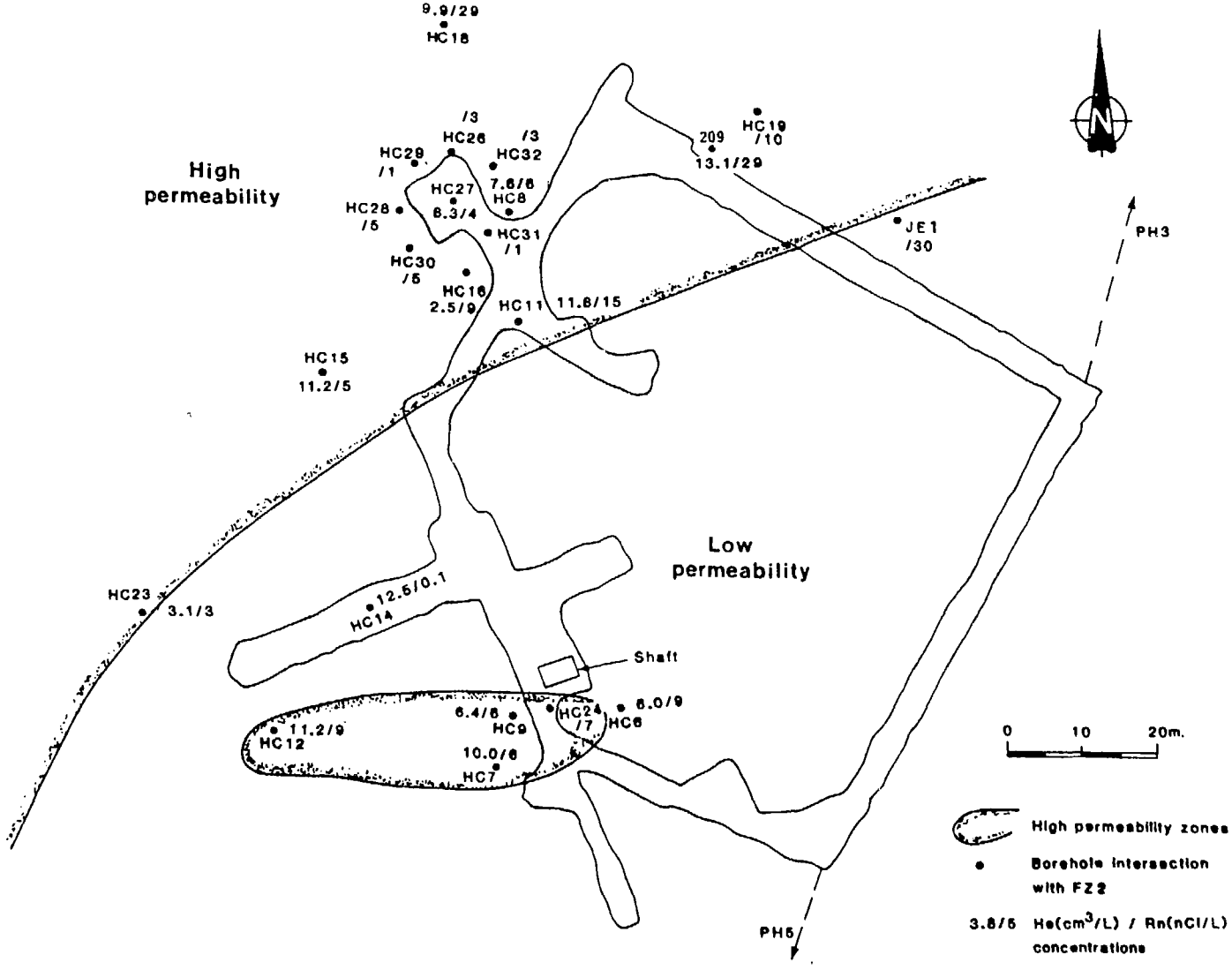

FIGURE 13: Concentrations of He and Rn in FZ2 Groundwaters from Boreholes Collared in the 240-m Level of the URL

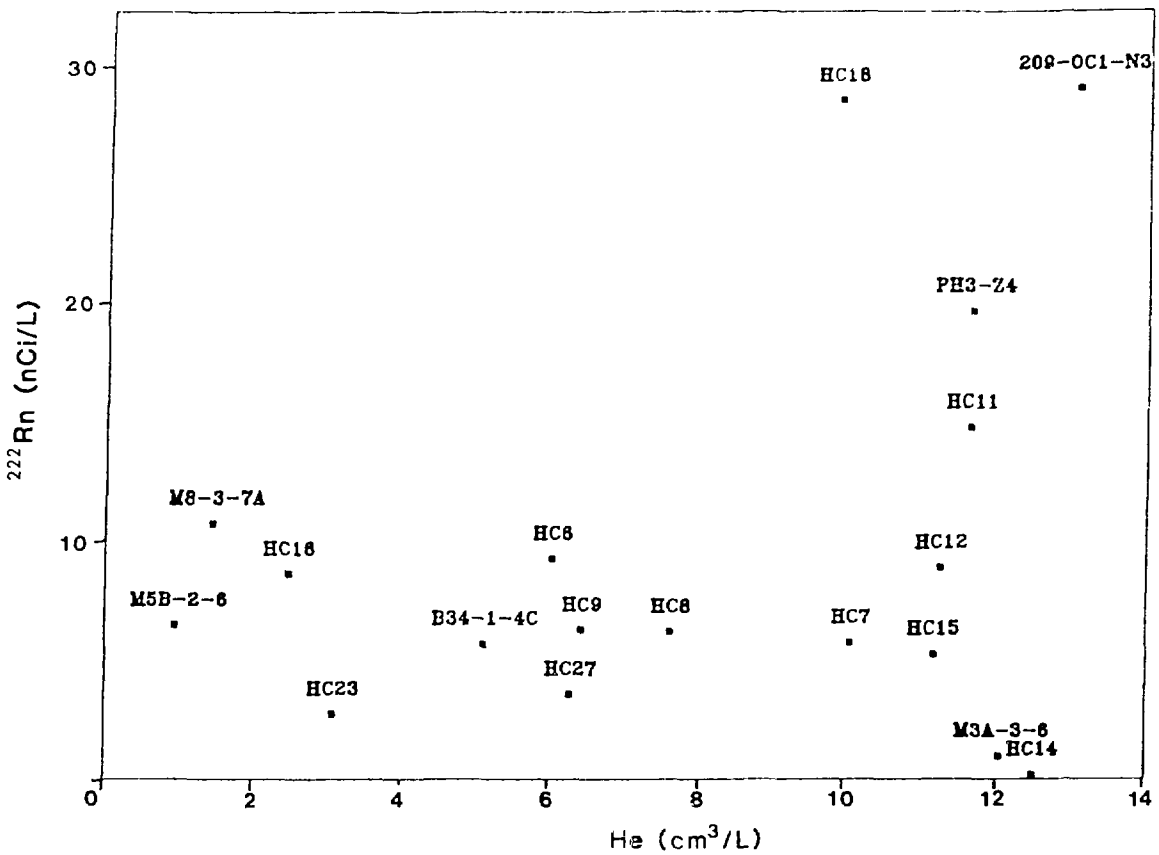

FIGURE 14: Variation of Rn with He Content for Groundwaters with Paired Measurements in the URL Lease Area and 240-m Level

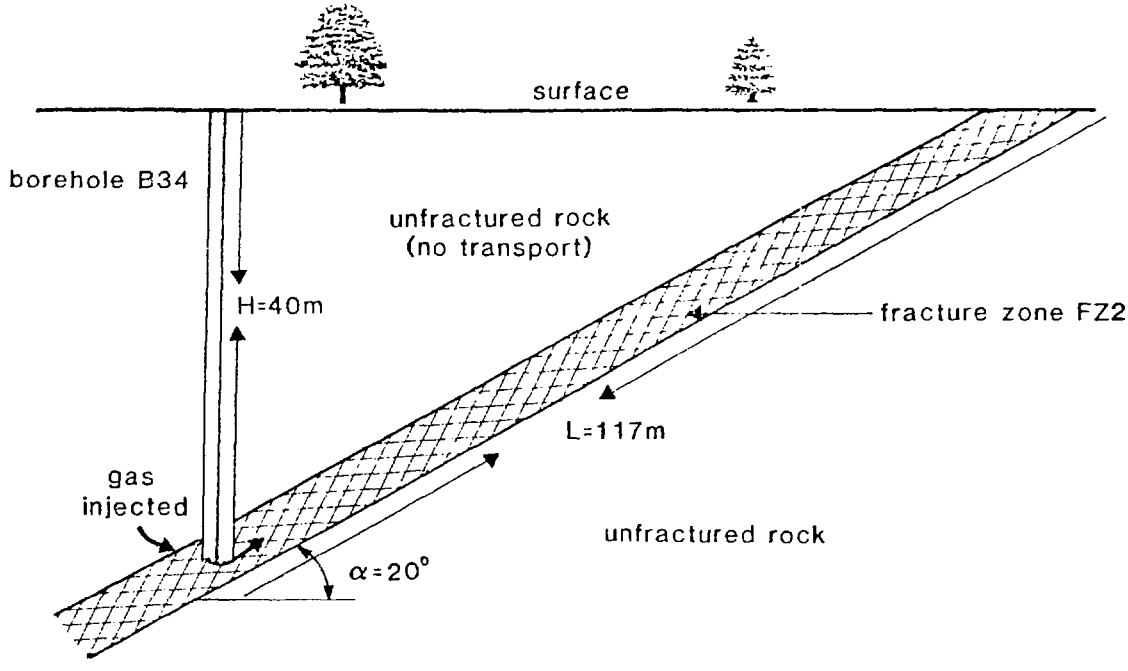

FIGURE 15: Gas Transport in a Fracture Zone in Low-Permeability Rock with no Overburden

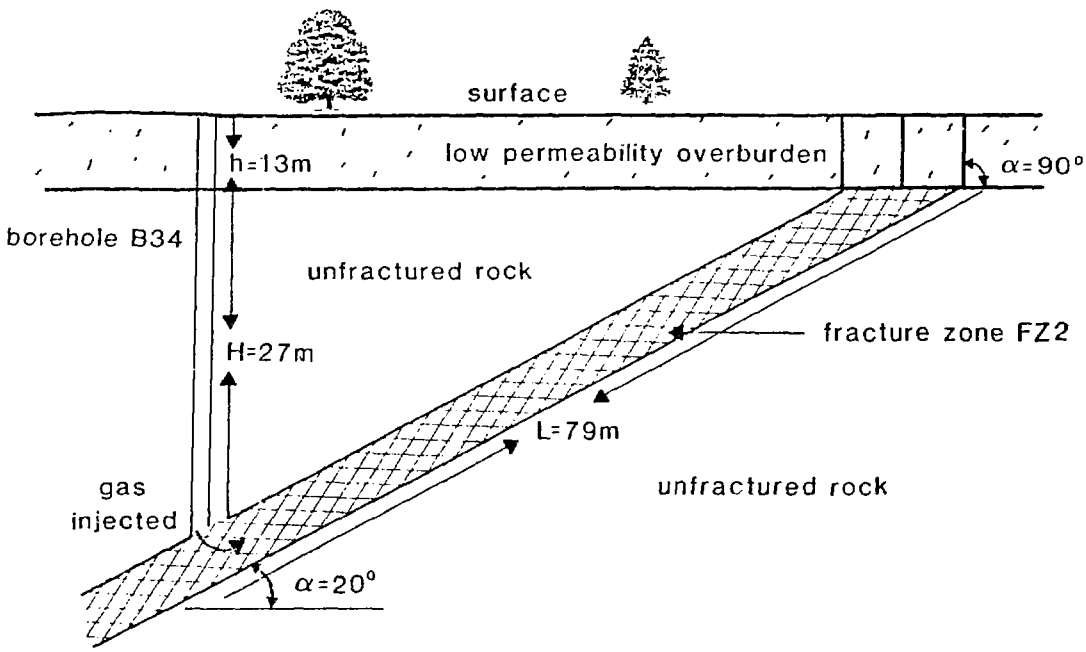

FIGURE 16: Gas Transport in a Fracture Zone with Low-Permeability Overburden

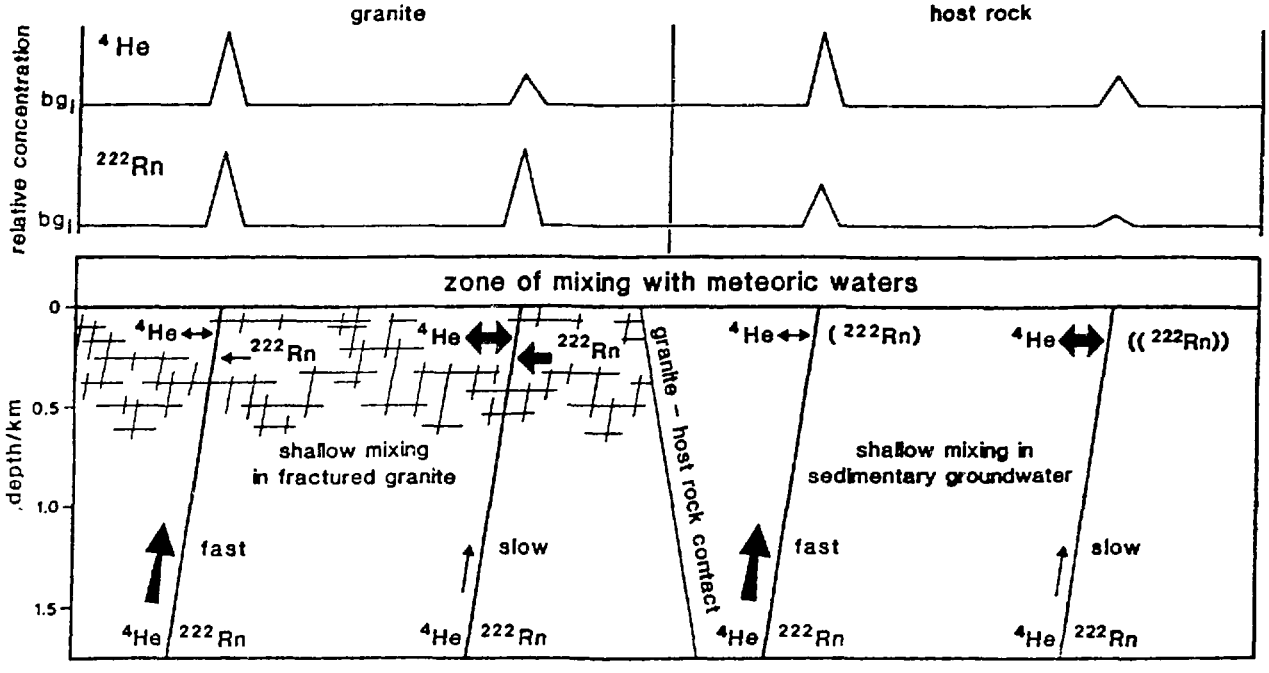

FIGURE 17: Comparison Between ^{4}He and ^{222}Rn Flux in Hydrothermally Driven Systems, and the Resultant Expression in Surface Waters Relative to Local Background (bg_l) (from Gregory and Durrance 1987)

APPENDIX A

SAMPLING AND ANALYTICAL TECHNIQUES

CONTENTS

The sampling and analytical techniques used generally follow those of Gregory and Durrance (1987) and Gregory (1987) but differ in some respects, as indicated below.

A.1 SOIL GAS SAMPLING

A.1.1 FIELD TECHNIQUES

The collection of soil gas in this project involved direct pumping of soil gas through a hollow probe driven 0.5 m into the ground. This equipment was supplied by the University of Exeter, U.K., and is essentially unchanged from that described by Gregory (1987). The sampling equipment (Figure A-1) consists of a hollow stainless steel probe, pounding hammer, a manifold assembly with a silicon rubber septum attachment and an extraction tool for the removal of the probe once sampling is completed. The hollow soil probe has a length of about 75 cm and an internal diameter of about 4 mm. At one end of the probe is a large-diameter collar, which acts as a receptor for the sampling manifold and a pounding block for the hammer. The pounding hammer consists of a steel rod that slides in a steel hammer head. The hammer is inserted into the probe with the end of the steel rod projecting out of the probe. This prevents the probe from blocking as it is hammered into the ground and also creates a gas space at the base of the probe. After sampling, an extraction tool, which is simply a steel wrench-like instrument, slots into grooves at the collar of the soil probe and is used to remove the probe from the ground. During sampling, the hammer is removed and a brass manifold inserted into the collar of the probe. The manifold is fitted with a Whitey toggle valve, a silicon rubber septum for gas sampling with a syringe and a 6-mm-diameter outlet for connecting the manifold to the sampling intake system.

The sample intake system consists of two Whitey toggle valves, a hand pump and a 60-mL plastic syringe, all interconnected by a Swagelok four-way "union cross." Figure A-1 illustrates the system. The hand pump is used to purge the probe of any atmospheric air (thereby allowing soil gas to be drawn in) and to evacuate the intake system. A large plastic syringe is used for drawing approximately 60 mL of sample gas out of the probe and for storing the sample for about 5 min to allow thoron (^{220}Rn) decay before filling the Lucas cell.

To sample all sites under similar conditions, a standardized procedure was adopted, as follows:

1) Pound soil probe approximately 0.5 m into ground.
2) Remove hammer from probe and insert sampling manifold with the intake system pressed into collar of probe.
3) With syringe valve and cell valve closed, open manifold valve.
4) Pump hand pump about twenty strokes to remove atmospheric air.
5) Close manifold valve and open syringe and cell valve.
6) Pump down inlet system to a reading of ~15 in. Hg* on vacuum gauge of hand pump. Check for leaks in system by observing gauge for a short period.

7) Close cell valve, open manifold valve and expand syringe to take 60-mL gas sample. Check gauge for indication of low permeability of soil zone.
8) Close the syringe valve when gauge pressure attains atmospheric level and wait for 5 min for thoron decay.
9) Meanwhile, insert disposable 10-mL plastic syringe fitted with tap through septum in manifold and withdraw 10-mL gas sample for helium analysis. Repeat with a second syringe.
10) With manifold valve and syringe valve closed, open cell valve to check that partial vacuum still exists. If not, pump cell down once more.
11) Open syringe valve and allow soil gas sample to fill cell.
12) Disconnect Lucas cell and seal it.
13) Allow cells to sit for three hours before counting.
14) Analyse duplicate helium samples on the mass spectrometer as soon as possible, usually within 24 h.

A.1.2 REMOVAL OF ATMOSPHERIC AIR IN SAMPLER

To determine the number of strokes of the hand pump required to remove trapped air in the system, a set of Lucas cells was filled sequentially with increasing number of hand strokes. The results are shown in Table A-1. It can be seen that after about 20 strokes, soil gas with a constant Rn activity was obtained.

TABLE A-1

EFFECT ON MEASURED RADON LEVELS OF REMOVAL OF ATMOSPHERIC AIR FROM SOIL GAS SAMPLING SYSTEM

Number of Strokes	Cell Count Rate (cpm)
5	124
10	138
15	175
20	191
25	202
30	195
35	197

A.1.3 EFFECT OF BAROMETRIC PRESSURE

One soil probe was installed permanently in each area to monitor the effects of changes in atmospheric pressure, etc., on soil gas Rn levels (He was not measured but was assumed to behave similarly to Rn). These results

---

* 1 in. Hg = 3.37685 kPa

are plotted against time in Figure A-2, together with daily readings of barometric pressure obtained by the meteorological station at Whiteshell Laboratories (B. Amiro, personal communication). It can be seen that there is some indication of an inverse relationship between barometric pressure and Rn level, as might be expected from factors known to control outgassing of the overburden.

A.2. ANALYTICAL METHODS

A.2.1 RADON

Radon analysis in soil gas samples was performed by counting Rn in equilibrium with its daughters in Lucas cells. These cells were made from PVC end caps for 2 in. (nominal) pipe with a Plexiglas window glued to the bottom and one or two Swagelok brass outlet tubes fitted to the top as a gas inlet/outlet. The cells were coated with a layer of silver-activated zinc sulphide to obtain a smooth coating on the inside of the end cap.

Lucas cells were filled in the field and counted in the laboratory at least three hours later when equilibrium with radon daughters had been reached. In this way, better precision on Rn activity was obtained than in the method using three one-minute counts immediately after sampling (Gregory 1987).

Because of slight variations in ZnS(Ag) coating thickness, instead of assuming a mean efficiency for all Lucas cells, each cell was calibrated by degassing a standard (NBS) ^{226}Ra solution into it at least once. A mean counting efficiency was determined for each cell and used to convert Rn (cpm) to Rn (dpm).* Radon levels are finally expressed as pCi/L of soil air.

As described in Section 1, thoron and daughters were prevented from entering the Lucas cell during filling at the sampling site by first drawing the soil gas into a 60-mL plastic syringe and letting it stand for 5 min before opening to the evacuated Lucas cell. This allows 97% of ^{220}Rn to decay and most of the longer-lived, non-gaseous daughter ^{212}Pb to become attached to container walls. The presence of thoron in soil air was verified by filling two Lucas cells sequentially from the same source, one with delay syringe, the other without, and noting that the decay in activity of the former followed that predicted by decay of Rn, whereas the latter contained an additional source.

A.2.2 HELIUM

To analyze helium in soil gases, a helium-leak detector was fitted with an external inlet system that allowed the introduction of the gaseous sample into the spectrometer under constant pressure. The electrical output of

---

* cpm - counts per minute
dpm - disintegration per minute

the leak detector was a leak indicator meter connected in parallel to a chart recorder. An external vacuum pump was also connected to the inlet system, enabling rapid evacuation of the system.

The helium analyzer for this project was the Veeco MS9AB mass spectrometer leak detector. It is solely designed for the detection of ions of mass-to-charge ratio of 4+. The principles of operation of the Veeco will not be described here.

The purpose of the external inlet system is to allow introduction of sample in small controlled quantities under constant pressure and for pre-concentration of helium in the sample. There are basically four sections to the inlet system: 1) evacuation valve and external vacuum pump, 2) injection port and sample clear valve, 3) the variable leak valve, and 4) U-trap.

Figure A-3 is a schematic diagram of the inlet system. Samples are introduced into the system through one port of a Swagelok union cross fitted with a silicon rubber septa and held in place by a Swagelok nut. Another port allows gas to flow to the variable leak valve and the remaining port is connected to the sample clear valve and external vacuum pump. The storage balloon acts as an expansion bladder and maintains a constant pressure supply to the variable leak valve. A 10-mL glass syringe was initially used in place of the balloon; however, it was found that the syringe plunger would often stick, resulting in a pressure drop at the leak valve inlet. This caused deflections on the chart recorder that were erratic and unmanageable. Replacing the syringe with the balloon apparatus resulted in a much more stable and manageable signal.

Between the inlet to the mass spectrometer and the leak valve there is a U-trap made out of a 3/8 in. (nominal) stainless steel tubing packed with activated charcoal. During analysis, the U-trap is immersed in dewar filled with liquid nitrogen. The use of the U-trap has two beneficial effects:

1) gases that can contaminate the spectrometer or degrade the filament, thereby reducing sensitivity, are removed (e.g., oxygen, water vapour, carbon dioxide); and

2) since the number of gas molecules entering the spectrometer has been reduced, the leak valve can be open to increase the throughput, thereby increasing the partial pressure of ^4He entering the spectrometer while maintaining a low pressure at the spectrometer head. The result is a dramatic increase in sensitivity.

When evacuating the inlet system, the U-trap by-pass valve is opened to prevent gases from being constantly pumped through the U-trap. In this way, the life of the activated charcoal within the trap is prolonged and overloading of the U-trap avoided. The pumpdown of the inlet system continues for approximately 15 min after completion of analysis. This allows any gases adsorbed onto the charcoal to degas and be pumped out of the system.

Laboratory air, presumed to be 5240-ppb He, along with 20- and 10-ppm He standards in nitrogen were used as calibration gases. Duplicate samples from each site were analysed with laboratory air samples bracketing each soil gas sample. Ten millilitres of gas were injected at a time, providing approximately 90% of output signal. Since the quantity of He in the soil gas can be either greater or less than that in air, the results were reported as He anomalies (Δ) rather than in absolute amounts. The He anomaly is calculated simply by subtracting 5240 ppb from determined quantities of He in the sample and expressing the result as a negative or positive value in ppb.

Figure A-4a shows an ideal He output signal on the chart recorder of the leak detector and a typical signal. An ideal output signal is rarely achieved because of factors such as pressure changes, electronic noise and amplifier drift. In many cases, there is an initial overshoot of the signal followed by a flat plateau region (Figure A-4b). The overshoot is due to the dynamic property of the constant-pressure inlet system and the adsorptive properties of the U-trap.

The linearity of the response of the mass spectrometer to helium is determined by separately injecting laboratory air, 10- and 20-ppm helium gas standards. A graph of the height of the deflection versus concentration of helium is shown in Figure A-5. Within experimental error, the relationship between the response of the mass spectrometer to concentration of helium is linear.

One particular problem of storing soil gas samples in plastic disposable syringes is the diffusion of helium through the seal and body of the syringe. To test the rate of diffusion of helium through the syringe, 10 mL of 10-ppm helium standard was stored for various periods of time and then analysed along with a fresh 10-ppm helium standard. Figure A-6 shows the results of these experiments. It was found that there was a diffusive loss of 0.33% per hour. In an attempt to minimize this problem, all helium samples were analysed as quickly as possible, usually within 24 h of sampling. Losses were therefore kept to within 10%.

A.2.3 SHALLOW GROUNDWATER

Sampling of groundwaters from the various overburden lithologies in the East Swamp area was possible through the multi-level piezometers using a battery-operated peristaltic pump. Each zone was pumped for several minutes, with the sampling tube about one metre above the intake screen, to draw fresh groundwater into the standpipe. The tube was then lowered so that this groundwater could be sampled. Steel cylinders (volume ~60 mL) for Rn and glass vessels (120 mL) for He were attached to the pump outlet to minimize degassing during sampling. The first attempts at sampling showed that some piezometer zones dried up before samples could be taken. It was also noted from one test of multiple sampling of a single zone, that Rn activity increased continuously with sampling, suggesting that stagnant water in the standpipe was still being sampled, even after 15 min of pumping. If this characteristic is common to all piezometer zones, then the Rn results obtained are likely to be suspect and be underestimates of the ambient Rn activity in the groundwater. Analysis of dissolved Rn was

performed by displacing the dissolved gases, under vacuum, into a Lucas cell through a vessel fitted with a glass-frit bubbler (Larocque and Gascoyne 1986).

Problems were experienced with the mass spectrometer at the time of the groundwater sampling and the samples taken for the analysis could not be analysed within seven days. The samples were therefore discarded and freeze-up prevented resampling for He.

A.2.4 SOILS

Several kilograms of soil from sites of varying radon activity were obtained from holes dug by hand to a depth of 0.45 to 0.60 m. The sites for these holes included the area of the Rn anomaly in the detailed soil gas survey, a completely flat area, and lower lying areas, one situated near the Rn anomaly. Care was taken to ensure that only soil from the floor of the hole was collected and that no soil from the side had fallen in. Each soil sample was placed into a clean Ziploc bag and sealed to prevent evaporation. Weighed amounts of each of eight sampled soils were placed in an oven at 113°C and dried to constant weight. The drying took five days and it was assumed that the change in weight was due to free water alone.

Several grams of the dried soils that were sampled for water content measurements were also sealed into clear plastic petri dishes with PVC cement and stored for eight weeks to allow ^{226}Ra to come to equilibrium with ^{214}Pb. The gamma emissions of this isotope were then measured using a Ge(Li) detector and the ^{226}Ra content of the soils was calculated.

REFERENCES

Gregory, R.G. 1987. Soil gas emanometry and hydrothermal mineralization in southwest England. Unpublished Ph.D. thesis, University of Exeter, Exeter, U.K.

Gregory, R.G. and E.M. Durrance. 1987. Helium, radon and hydrothermal circulation associated with the Carnmenellis radiothermal granite of southwest England. Journal of Geophysical Research 92 (B12), 12567-12586.

Larocque, J.P.A. and M. Gascoyne. 1986. A survey of the radioactivity of surface water and groundwater in the Atikokan area, northwestern Ontario. Atomic Energy of Canada Limited Technical Record, TR-379.*

---

* Unpublished report available from SDDO, AECL Research, Chalk River Laboratories, Chalk River, Ontario K0J 1J0.

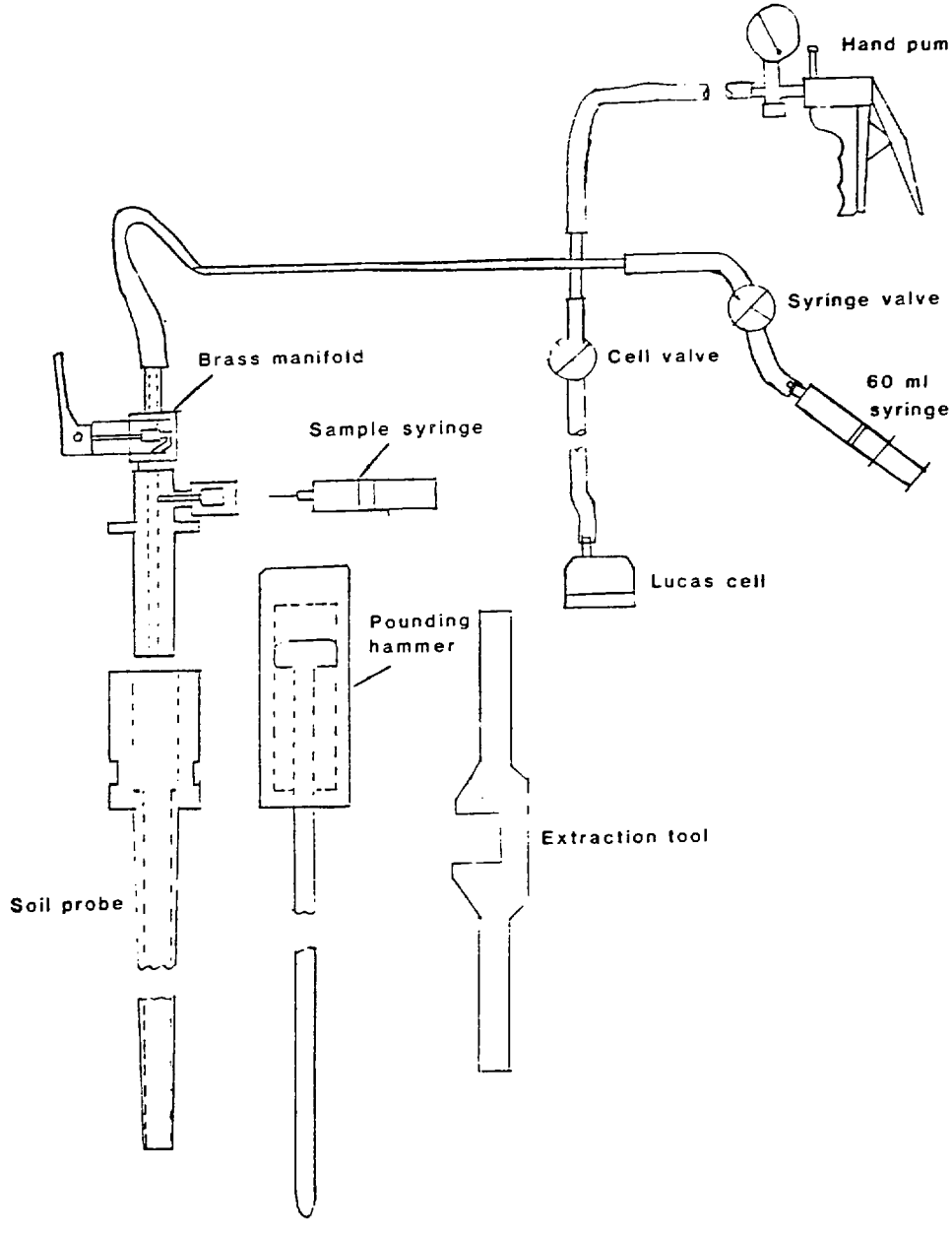

FIGURE A-1: Schematic Diagram of the Soil Gas Sampling Equipment

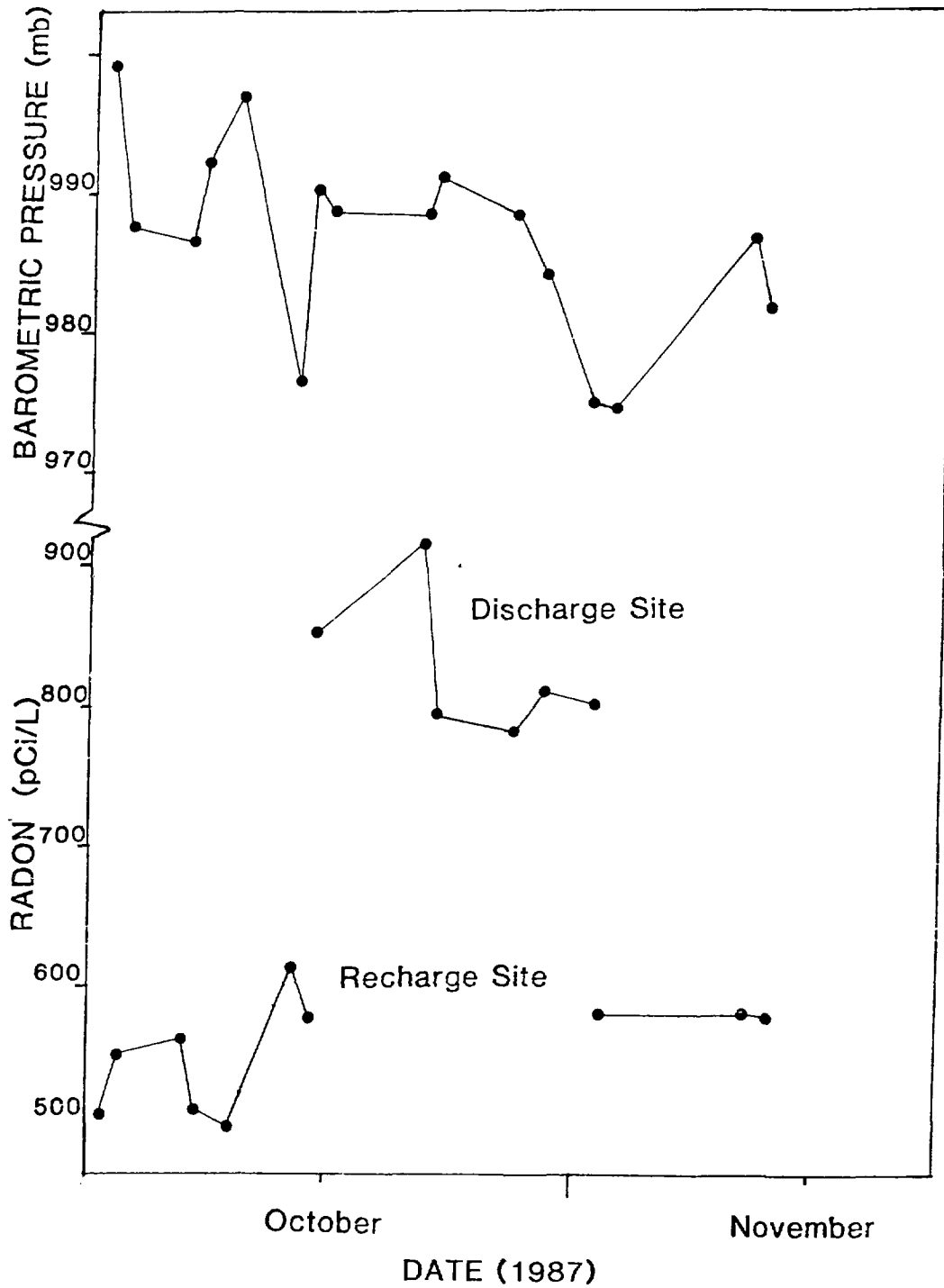

FIGURE A-2: Variation of Radon Content of Soil Gases for the Two Standard Sites with Barometric Pressure Determined at Whiteshell (1 b = 100 kPa)

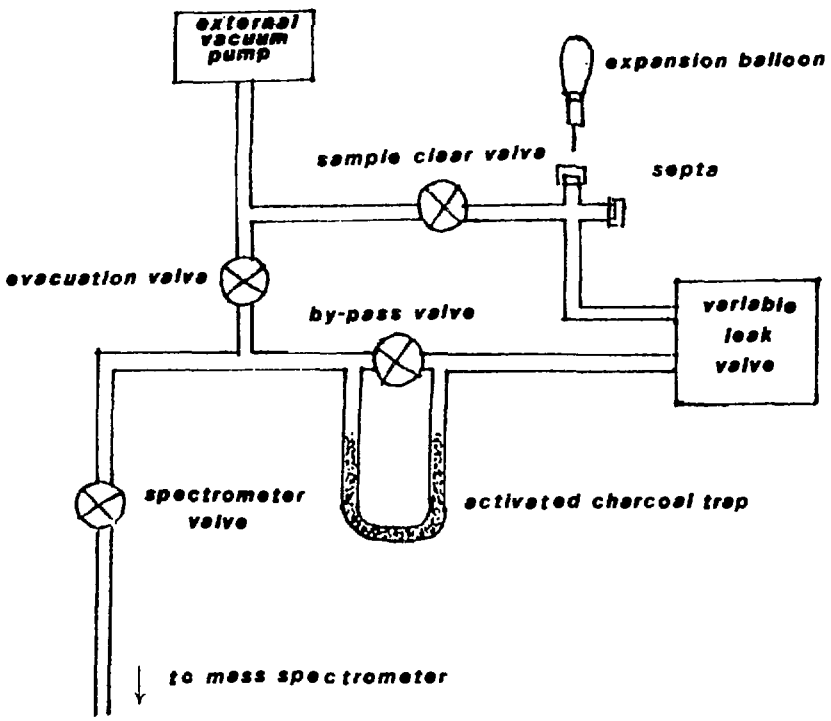

FIGURE A-3: Sample Inlet System for the Helium Mass Spectrometer

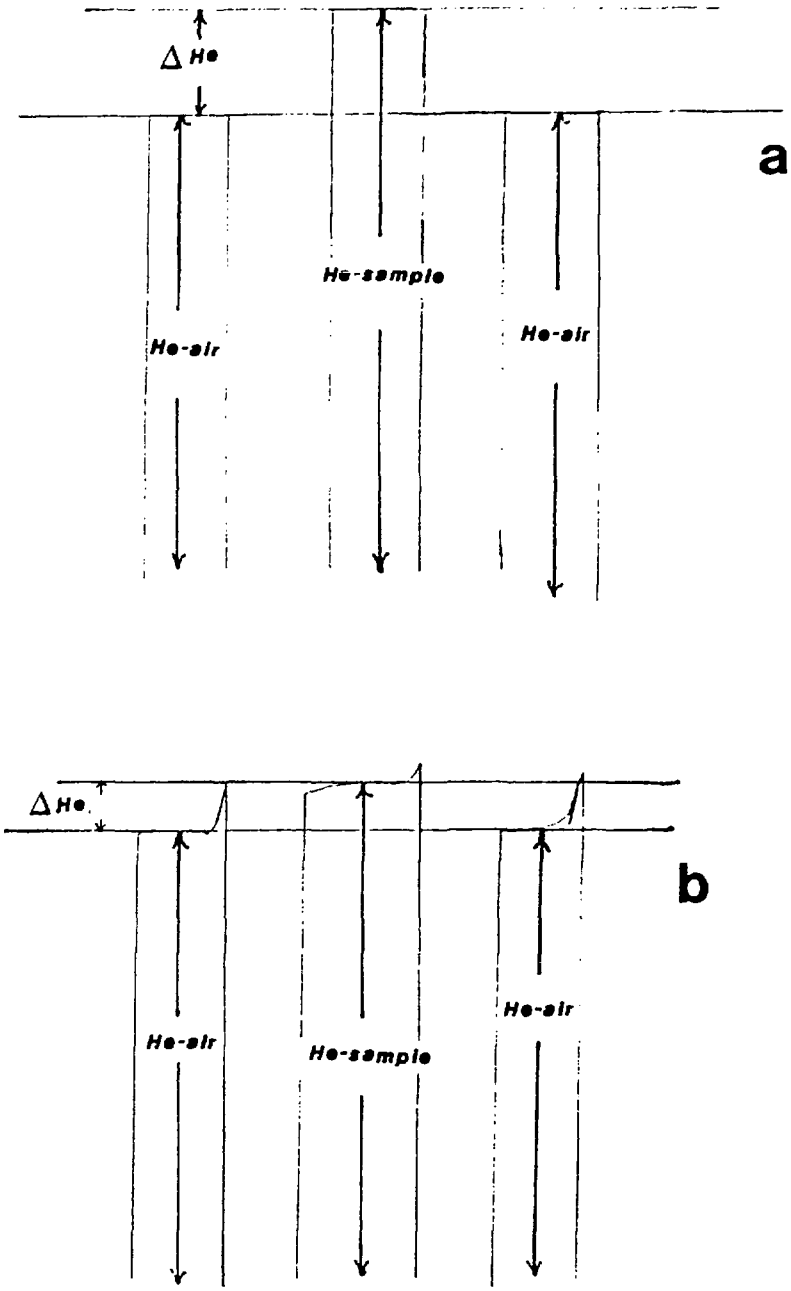

FIGURE A-4: Examples of Helium Signals on the Mass Spectrometer: a) Idealized, and b) Typical Showing Initial Spikes

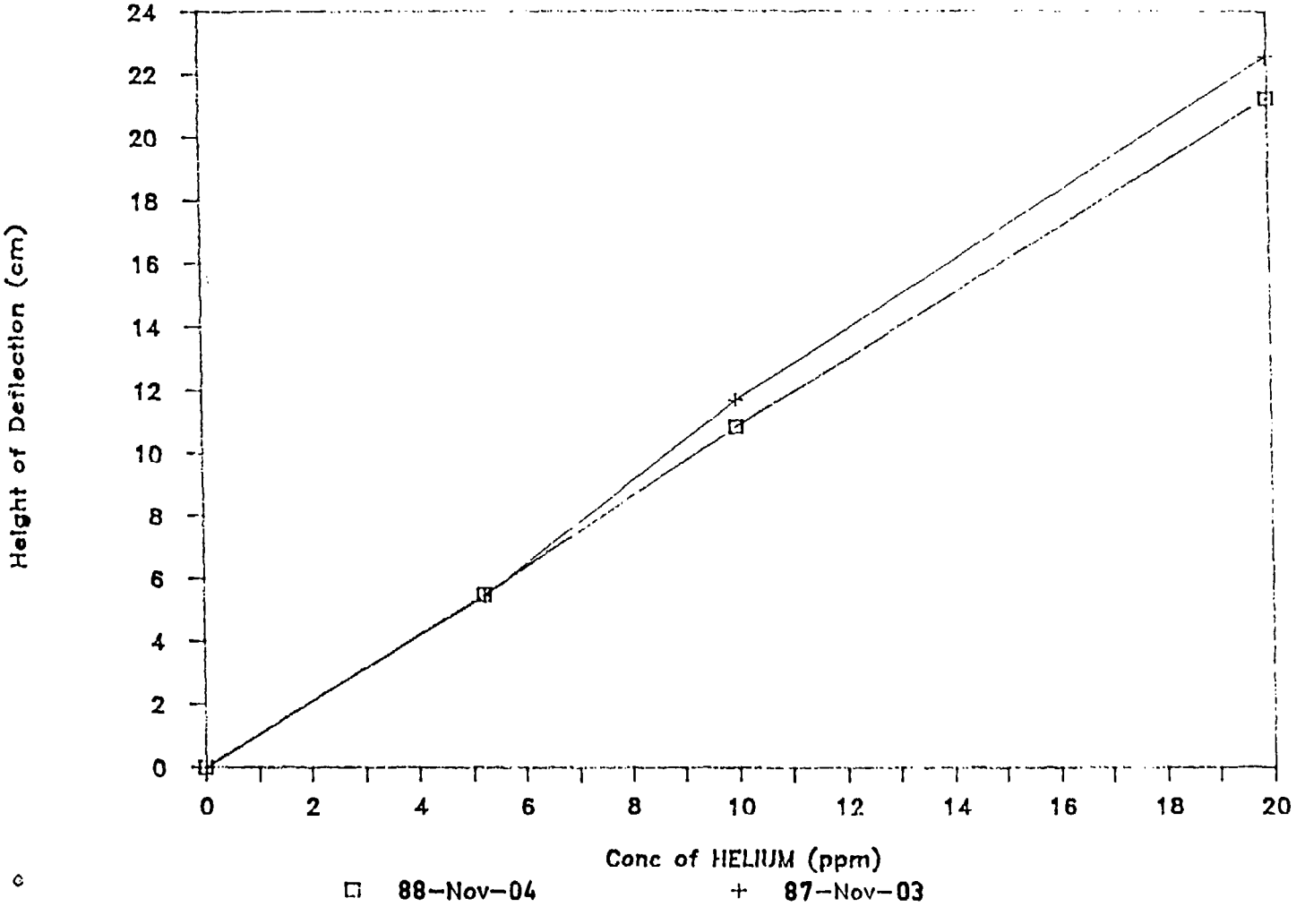

FIGURE A-5: Test for Linearity of Response of the Mass Spectrometer to Various Concentrations of Helium in Nitrogen

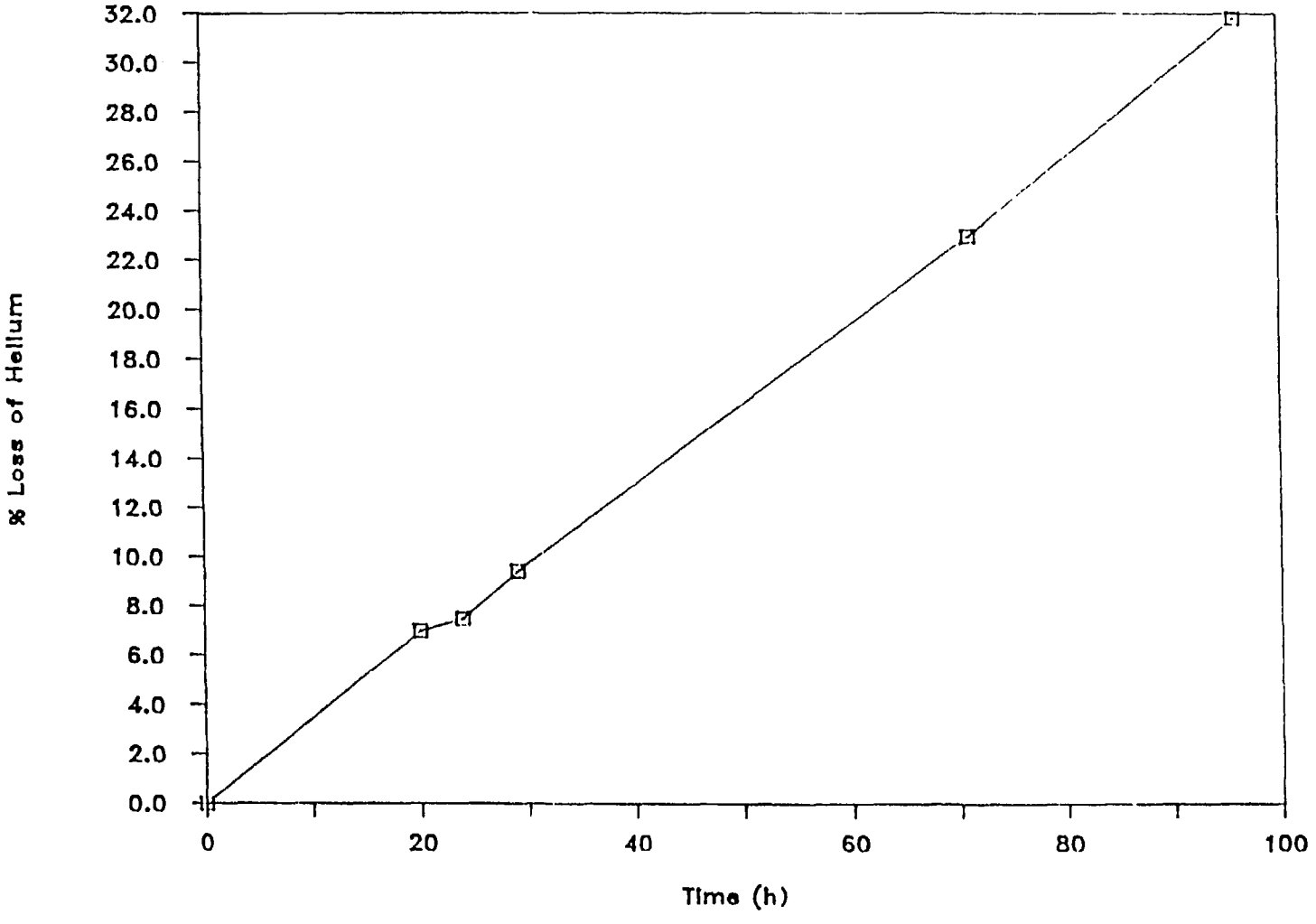

FIGURE A-6: Determination of the Leak Rate of Helium from 10-mL Plastic Syringes Fitted with Taps

APPENDIX B

DERIVATION OF MODELLING EQUATIONS

CONTENTS

NOMENCLATURE

Latin Symbol	Description	Dimension
b	fracture width	L
b_{eff}	effective fracture width over fracture zone	L
d	distance between adjacent fractures	L
g	acceleration of gravity	$L \cdot T^{-2}$
H, H_j	vertical height of the (jth) rock layer	L
$H_{over,j}$	vertical distance between the top of the jth rock layer and the surface	L
H_{TOT}	vertical distance from the point of injection to the rock surface	L
k	bulk permeability of the fracture zone	L^2
k_f	permeability of a single fracture	L^2
K	bulk hydraulic conductivity	$L \cdot T^{-1}$
L	length of the fracture zone	L
n	fracture frequency per unit length	L^{-1}
P_c	capillary pressure	$M \cdot L^{-1} \cdot T^{-2}$
P_H	hydrostatic pressure at point of injection	$M \cdot L^{-1} \cdot T^{-2}$
P_I	injection pressure of gas	$M \cdot L^{-1} \cdot T^{-2}$
P_T	threshold pressure to initiate gas flow	$M \cdot L^{-1} \cdot T^{-2}$
P	pressure	$M \cdot L^{-1} \cdot T^{-2}$
q	volumetric rate of flow per unit area	$L \cdot T^{-1}$
R_1, R_2	radii of curvatures of the meniscus between two fluids	L
s	coordinate along a fracture	L
t	time	T
t_b	breakthrough time for gas for the gas	T
T	temperature	K
v	velocity	$L \cdot T^{-1}$

Greek Symbols	Description	Dimension
α	see ϕ	
θ	contact angle at gas-water meniscus	-
ρ	density	$M \cdot L^{-3}$
μ	dynamic viscosity	$M \cdot L^{-1} \cdot T^{-1}$
$\Delta\rho$	difference between water and gas densities ($\Delta\rho = \rho_w - \rho_g$)	$M \cdot L^{-3}$
σ	interfacial tension at meniscus between two fluids	$M \cdot T^{-2}$
α	angle of the fracture zone with the horizontal plane	-
ϕ	pressure head $\phi = P + \rho gz$	$M \cdot L^{-1} \cdot T^{-2}$
ξ	local coordinate of the gas-water interface in the s direction	L

Subscripts

g	gas
o	s = 0
L	s = L
w	water

B.1 MODELLING APPROACH

The injection test is conceptualized as shown in Figure B-1, i.e., helium gas is injected through borehole B34 into the fracture zone FZ2 that the borehole intersects. The permeability of the fracture zone is much greater than that of the surrounding rock, so transport of gas outside the fracture zone is neglected.

Equations are initially developed for the transport properties of a single open fracture and then are related to the bulk properties of the fracture zone of the rock, derived from experimental measurements. Equations are derived for

- the threshold injection pressure required to initiate flow;
- the breakthrough time of the gas, i.e., the time required for the initial arrival of gas at the surface; and
- the velocity of the gas after breakthrough, and its volumetric flow rate, as a function of injection pressure.

The derivation of the equations is based on the analysis given in Braester and Thunvik (1982), and Thunvik and Braester (1987).

In Section B.4, the equations developed are generalized for modelling layered rock, or rock with overburden.

B.2 DERIVATION OF EQUATIONS FOR A SINGLE OPEN FRACTURE

B.2.1 THRESHOLD PRESSURE

Purpose: To calculate the injection pressure required to initiate gas flow in a single open fracture.

Derivation of Equation:

P_T = threshold pressure
= critical pressure to initiate gas flow in an ideal open fracture
= capillary pressure + hydrostatic pressure at point of injection
= $P_c + P_H$. (B.1)

The Laplace formula relates the capillary pressure to the interfacial tension, σ, and the radii of curvature of the meniscus between the two fluids:

$$P_c = \sigma \left(\frac{1}{R_1} + \frac{1}{R_2}\right) \quad . \tag{B.2}$$

For a fracture plane, $R_2 \rightarrow \infty$ areal

$$P_c = \frac{\sigma}{R_1} \quad . \tag{B.3}$$

The radius of curvature of the meniscus between the gas and the water, R_1, can be related to the fracture width, b, and to the contact angle, θ ($\theta < 90°$, defining the wetting fluid):

$$R_1 = b/(2 \cos \theta) \quad . \tag{B.4}$$

which substituted into Equation (B.3) yields

$$P_c = (2\sigma \cos \theta)/b \quad . \tag{B.5}$$

The contact angle is a property of the couple of the fluid and the solid boundary. As no data are available for the contact angle θ, we will assume the value leading to the maximum P_c, i.e., $\cos \theta = 1$:

$$P_c = \frac{2\sigma}{b} \quad . \tag{B.6}$$

Substituting into Equation (1) yields

$$P_T = \frac{2\sigma}{b} + P_H \quad , \text{ or} \tag{B.7}$$

$$= \frac{2\sigma}{b} + \rho_w g H \tag{B.8}$$

B.2.2 BREAKTHROUGH TIME OF GAS

Purpose: To calculate the breakthrough time for the gas to reach the surface, i.e., the time required to displace the water in a single open fracture initially saturated with water.

Derivation of Equation:

If gas at a pressure P_I is injected into a fracture in the s direction, inclined at an angle α with the horizontal (see Figure B-2), then

$s = 0$ at the point of injection,
$s = L$ at the rock surface, and
$s = \xi(t)$ at the gas-water interface at time t.

The gas will be treated as incompressible. Its density and viscosity will be approximated by the average density and viscosity between the point of injection and the liquid-water interface surface. (If the gas is considered compressible, a numerical integration of the equations is required.) The ratio of the pressure drop in the gas phase to the injection pressure is

$$\frac{\Delta P_g}{P_T} = \frac{\rho_g g H}{\rho_w g H + P_c}$$

$$\simeq \frac{\rho_g}{\rho_w} \text{ where } \rho_w g H >> P_c \quad ,$$

ΔP_g = pressure drop in the gas phase between the point of injection and the surface, prior to breakthrough. Hence, treating the gas as incompressible is a good approximation when the hydraulic pressure at the point of injection is small relative to the capillary pressure, and a poor approximation when it is not.

The equations of motion are (Poiseuille's Law)

$$v_g = - \frac{k_f}{\mu_g} \frac{\partial \phi_g}{\partial s}$$

$$v_w = - \frac{k_f}{\mu_w} \frac{\partial \phi_w}{\partial s} \quad . \tag{B.9}$$

The equations for conservation of mass are

$$\frac{\partial v_g}{\partial s} = 0$$

$$\frac{\partial v_w}{\partial_s} = 0 \quad . \tag{B.10}$$

Substituting Equations (B.9) into Equations (B.10) gives

$$\frac{\partial^2 \phi_g}{\partial s^2} = 0 \qquad 0 \leq s \leq \xi \tag{B.11}$$

$$\frac{\partial^2 \phi_w}{\partial s^2} = 0 \qquad \xi \leq s \leq L \tag{B.12}$$

where $\phi_i = P_i + \rho_i g z$ and i denotes the gas (i = g) or water phase (i = w).

Integrating Equations (B.11) and (B.12) under boundary and initial conditions

$$s = 0 \quad \phi_g (0) \equiv \phi_{go} = P_I \quad \text{(at the point of injection to the fracture zone)} \tag{B.13}$$

$$s = \xi \quad \phi_g (\xi) \equiv \phi_{g\xi} , \quad \phi_w = \phi_{w\xi} \text{ (at the liquid gas face)} \tag{B.14}$$

$$x = L \quad \phi_w (L) \equiv \phi_{wL} = 0 \text{ (at the surface)}, \tag{B.15}$$

we obtain

$$\phi_g = \phi_{go} + \frac{\phi_{g\xi} - \phi_{go}}{\xi} s \tag{B.16}$$

$$\phi_w = \phi_{w\xi} + \frac{\phi_{wL} - \phi_{w\xi}}{L - \xi} (s - \xi) \quad . \tag{B.17}$$

The linearity of Equation (B.10) in s shows that the fluid velocity in each of the two regions, gas and water, is constant over the domain occupied by the respective fluid. Moreover, at the gas-water interface, the velocities of the two fluids are equal. It follows that at any instant the velocities are equal over the entire flow domain, i.e., $v_g = v_w$.

Substitution of Equations (B.16) and (B.17) into Equations (B.9) yields

$$v_g = \frac{k_f}{\mu_g} \frac{\phi_{go} - \phi_{g\xi}}{\xi} \tag{B.18}$$

$$v_w = \frac{k_f}{\mu_w} \frac{\phi_{w\xi} - \phi_{wL}}{L - \xi} \tag{B.19}$$

or, in terms of pressure,

$$v_g = \frac{k_f}{\mu_g} \frac{P_{go} - P_{g\xi} - \rho_g g\xi \sin \alpha}{\xi} \tag{B.20}$$

$$v_w = \frac{k_f}{\mu_w} \frac{P_{w\xi} - P_{wL} - \rho_w g(L - \xi) \sin \alpha}{L - \xi} \quad . \tag{B.21}$$

Setting $v_w = v_g$ and adding gives

$$v_g = \frac{k_f}{\mu_g} \frac{P_{go} - P_{wL} - (P_{g\xi} - P_{w\xi}) - gL\rho_w \sin \alpha + g\Delta\rho\xi \sin \alpha}{\xi + \frac{\mu_w}{\mu_g}(L - \xi)} \tag{B.22}$$

where $\Delta\rho = \rho_w - \rho_g$ is the density difference between water and gas.

The difference in pressure between the gas and the water, $P_g - P_w$ at the interface equals the capillary pressure, P_c. Substituting $P_c = P_{g\xi} - P_{w\xi}$ yields

$$v_g = \frac{k_f}{\mu_g} \frac{P_{go} - P_{wL} - P_c - g\rho_w L \sin \alpha + g\Delta\rho\xi \sin \alpha}{\xi + \frac{\mu_w}{\mu_g}(L - \xi)} \tag{B.23}$$

$$= \frac{d\xi}{dt}$$

i.e., the velocity of the gas/liquid interface.

Integrating Equation (B.23) with initial condition $\xi = 0$ at $t = 0$, and defining $\Delta P = P_{go} - P_{wL} - P_c$ (B.24)

$= P_I - P_c$ (from Equations (B.13) and (B.15)) (B.25)

gives

$$t = \frac{\mu_g}{k_f} \frac{1}{g\Delta\rho \sin \alpha} \left(\frac{\mu_w}{\mu_g} L - \frac{(1 - \frac{\mu_w}{\mu_g})(\Delta P - \rho_w g L \sin \alpha)}{g\Delta\rho \sin \alpha} \right)$$

$$\cdot \left[\ln \left(1 + \frac{g\Delta\rho\xi \sin \alpha}{\Delta P - \rho_w g L \sin \alpha} \right) \right] + \left(1 - \frac{\mu_w}{\mu_g} \right) \xi \qquad \text{(B.26)}$$

for $\alpha \neq 0$.

The position of the gas/liquid interface at any time can be calculated by iteratively solving Equation (B.26) for ξ.

The breakthrough time, t_b, is obtained for $\xi = L$ in Equation (B.26). Using also the relationship $L = H/(\sin \alpha)$ yields

$$t_b = \frac{\mu_g}{k_f} \frac{1}{g\Delta\rho \sin^2 \alpha} \left[\left(\frac{\mu_w}{\mu_g} H - \frac{(1 - \frac{\mu_w}{\mu_g})(\Delta P - \rho_w g H)}{g\Delta\rho} \right) \right]$$

$$\cdot \left[\ln \left(1 + \frac{g\Delta\rho H}{\Delta P - \rho_w g H} \right) \right] + (1 - \frac{\mu_w}{\mu_g}) H \Bigg] \quad . \qquad \text{(B.27)}$$

B.2.3 VELOCITY OF GAS AFTER BREAKTHROUGH

Purpose: To calculate the velocity of the gas after complete displacement of the water from the fracture, i.e., the injection flow rate needed to maintain steady-state flow.

Derivation of Equation:

Equation (B.23) gives the velocity of the gas as a function of the length of the displacement ξ. After the complete displacement of the water from the fracture, i.e., for $\xi = L$ in Equation (B.23), we obtain the gas velocity through the gas-saturated fracture:

$$v_{gL} = \frac{k_f}{\mu_g} \frac{P_{go} - P_{wL} - g\rho_g L \sin \alpha}{L} \quad . \qquad \text{(B.28)}$$

Using the relationship $H = L \sin\alpha$ yields

$$v_{gL} = \frac{k_f}{\mu_g} \frac{P_{go} - P_{wL} - g\rho_g H}{L} \quad . \tag{B.29}$$

Substituting the value given in Equations (B.13) and (B.15) for the boundary conditions P_{go} and P_wL yields

$$v_{gL} = \frac{k_f}{\mu_g} \frac{P_I - g\rho_g H}{L} \quad . \tag{B.30}$$

B.3 RELATING THE PROPERTIES OF A SINGLE FRACTURE TO THE PROPERTIES OF BULK FRACTURED ROCK

B.3.1 PERMEABILITY, FRACTURE WIDTH AND FRACTURE SPACING

From the solution of the Navier-Stokes equation for the flow between two parallel plates, the permeability of a single fracture, k_f, is given by

$$k_f = \frac{b^2}{12} \tag{B.31}$$

where b is the fracture width.

The permeability of the fracture zone obtained from field tests, such as packer tests, will be an average value of the permeability of the fracture zone, i.e., of the bulk permeability of the fracture network in this volume.

The relationship between the bulk fracture zone permeability (k) and the permeability in the individual fractures (k_f) can be calculated from the geometrical parameters of the fracture network. An idealized network consisting of three orthogonal isotropic fracture systems is considered (Figure B-3), in which the orientation, spacing and width of fractures are assumed to be constant over the flow domain.

Averaging the fracture permeability over the bulk volume of this configuration and assuming flow in two sets of orthogonal fractures, the permeability, k, of the fracture zone is obtained:

$$k = b^3/6d \qquad \text{or} \qquad b = \sqrt[3]{6kd} \quad . \tag{B.32}$$

The parameter d can be obtained by inspection of drill cores.

The bulk permeability of the fracture zone, k, and its bulk hydraulic conductivity, K, are related by

$$k = \frac{K\mu_w}{\rho_w g} \quad . \tag{B.33}$$

B.3.2 THE THRESHOLD PRESSURE

The threshold pressure required to initiate gas flow in a single open fracture is given by

$$P_T = \frac{2\sigma}{b} + P_H \quad . \tag{B.7}$$

P_H, the hydrostatic pressure, can be calculated from the relationship $P_H = \rho_w g H$ and σ, the interfacial tension, can be obtained from the literature.

The parameter b, the fracture width, will be statistically distributed and d, the fracture spacing, will be neither constant nor isotropic in the fracture zone. In reality, for slow injection at low pressures, gas flow will take place only in the largest fractures (i.e., those having the lowest capillary pressure); for faster injection at higher pressure, gas flow will be initiated in smaller fractures and the average b of gas-conducting fractures will be smaller.

For the gas injection experiments, an effective value of b, b_{eff}, can be calculated from the experimentally determined permeability or hydraulic conductivity of the fracture zone, and the average fracture spacing within this zone (Equations (B.32) and (B.33)). This will probably underestimate b_{eff} (i.e., undervalue the importance of large fractures) and overestimate P_T.

B.3.3 BREAKTHROUGH TIME OF GAS

For each value of the injection pressure, the corresponding breakthrough time may be calculated by substituting b_{eff} for b in Equation (B.27), and using the value of k_f corresponding to b_{eff}.

B.3.4 VOLUMETRIC FLOW RATE OF GAS AFTER BREAKTHROUGH

The volumetric flow rate of the gas after breakthrough is obtained by multiplying the velocity of the gas after breakthrough (Equation (B.30)) by the area of the fractures. For the fracture configuration in Figure B-3 with n fractures per metre in each direction (n = 1/d) and assuming flow in two sets of orthogonal fractures, the volumetric rate of flow per unit (bulk) area of the fracture zone is given by

$$q_g = v_g 2nb = v_g \frac{2b}{d} \quad . \tag{B.34}$$

Substituting v_{gL} from Equation (B.29) for v_g yields

$$q_g = \frac{2bk_f}{dL\mu_g} \left(P_{go} - P_{WL} - g\rho_g H\right) \quad . \tag{B.35}$$

Substituting $b = b_{eff}$ and $k_f = \frac{b_{eff}^2}{12}$ (from Equation (28)) gives

$$q_g = \frac{1}{6} \frac{b_{eff}^3}{dL\mu_g} \left(P_{go} - P_{WL} - g\rho_g H\right) \tag{B.36}$$

$$= \frac{1}{6} \frac{b_{eff}^3}{dL\mu_g} \left(P_I - g\rho_g H\right) \tag{B.37}$$

using the values given in Equations (B.13) and (B.15) for the boundary conditions P_{go} and P_{WL}.

Equation (B.37) can also be used to calculate the injection pressure required to maintain a required volumetric flow rate, q_g.

B.4 TRANSPORT THROUGH LAYERED ROCK (OR ROCK + OVERBURDEN)

If there are n layers of rock with different properties (e.g., d, k, K) and/or fracture orientation (α), the system may be simulated by modelling each layer individually and matching the boundary conditions at each interface. The total breakthrough time is the sum of the breakthrough times for each layer.

B.4.1 THRESHOLD PRESSURE

The threshold pressure is the hydraulic pressure at the point of injection plus the largest capillary pressure along the flow path, i.e.,

$$P_T = H_{TOT}\rho_w g + P_c(max),$$

where

H_{TOT} = the vertical distance from the point of injection to the rock surface, and

$P_c(max)$ = the largest capillary pressure in any rock layer.

B.4.2 BREAKTHROUGH TIME AND FLOW RATE

The equations developed in Sections B.2 and B.3 are applicable, except that the generalized form of the boundary conditions P_{go} and P_{WL} must be used, i.e., Equation (B.24) instead of (B.25), Equation (B.29) instead of (B.30), and Equation (B.36) instead of (B.37).

Equations (B.25), (B.30) and (B.37) then become (B.25′), (B.30′) and (B.37′) respectively for the jth layer of rock:

$$\Delta P = P_{go} - \rho_w g H_{over,j} - P_c \qquad (B.25')$$

$$v_{gL} = \frac{k_f}{\mu_g L}\left(P_{go} - \rho_w g H_{over,j} - g\rho_g H_j\right) \qquad (B.30')$$

$$q_g = \frac{1}{6}\frac{b_{eff}^3}{dL\mu_g}\left(P_{go} - \rho_w g H_{over,j} - g\rho_g H_j\right) \qquad (B.37')$$

where

H_j = vertical height of the jth layer of rock,
$H_{over,j}$ = vertical distance between the top of the jth rock layer and the surface,
$P_{go} = P_I - g\rho_g H_{under,j}$,

where

$H_{under,j}$ = vertical distance from the point of injection up to the bottom of the jth rock layer (the second term of P_{go} is very small and can be neglected).

These equations may be used to model transport through several layers of fractured rock or through a layer of fractured rock and its overburden.

B.5 PARAMETER VALUES

B.5.1 VALUES OBTAINED FROM THE LITERATURE

The fluids in the experiment are helium and water. The following material properties were used in the calculations:

temperature (T)	10°C
water viscosity (μ_w)	1.307×10^{-3} N·s/m²
water density (ρ_w)	0.999×10^3 kg/m³
helium viscosity (μ_g)*	1.90×10^{-5} N·s/m²
helium density (ρ_g)	0.37 kg/m³
helium-water interfacial tension (σ) (value for hydrogen; value for helium not available)	0.07422 N/m
acceleration of gravity (g)	9.81 m/s²

* at T = 10°C, P = 0.2 MPa (average pressure of gas in fracture zone)

B.5.2 EXPERIMENTALLY DETERMINED AND DERIVED PARAMETERS

1. Geometry parameters:
   H_{TOT} = vertical distance from point of injection to surface
   = 40 m (40 m rock, or 27 m rock + 13 m overburden)
   α = angle of inclination of fracture zone with horizontal
   = 20° (rock); 0° (overburden)
   L = length of fracture zone (calculated from $L = H/\sin \alpha$)

2. Hydrogeological parameters:
   P_H = hydraulic pressure at point of injection (Pa), calculated from $P_H = \rho_w g H_{TOT}$
   K = bulk hydraulic conductivity (from packer tests)
   = 2×10^{-6} m/s (rock); 2×10^{-9} m/s (overburden)
   d = average fracture spacing in fracture zone
   = test length between packers (for rock)
   = 27 m (rock); 1 m (overburden)
   b_{eff} = effective value of crack width (m), calculated from K and d
   k = bulk permeability of fracture zone (m^2), calculated
   k_f = permeability of single fracture (m^2)

3. Parameters measured in injection tests (for comparison with calculated values):
   P_T = threshold pressure for injection (Pa)
   t_b = breakthrough time of gas (s)
   q_g = steady-state flow of gas (m^3/s, per square metre of the fracture zone) and corresponding pressure P_I (Pa)

REFERENCES

Braester, C. and R. Thunvik. 1982. An analysis of the conditions of gas migration from a low-level radioactive waste repository. Swedish Nuclear Fuel Supply Co., Division KBS Report, SKBF-KBS-TR-83-21.

Thunvik, R. and C. Braester. 1987. Calculation of gas migration in fractured rock. Swedish Nuclear Fuel and Waste Management Co. Technical Report, KBS-TR-87-18.

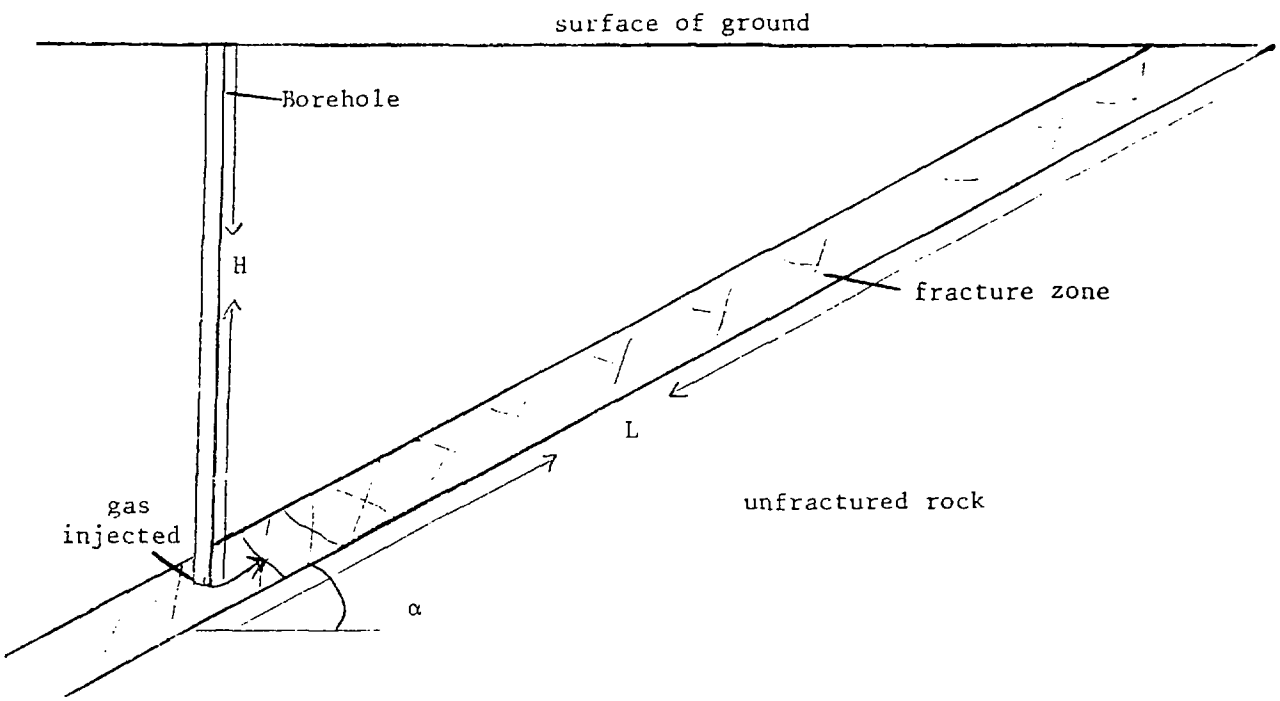

FIGURE B-1: Conceptualization of Gas Injection Test

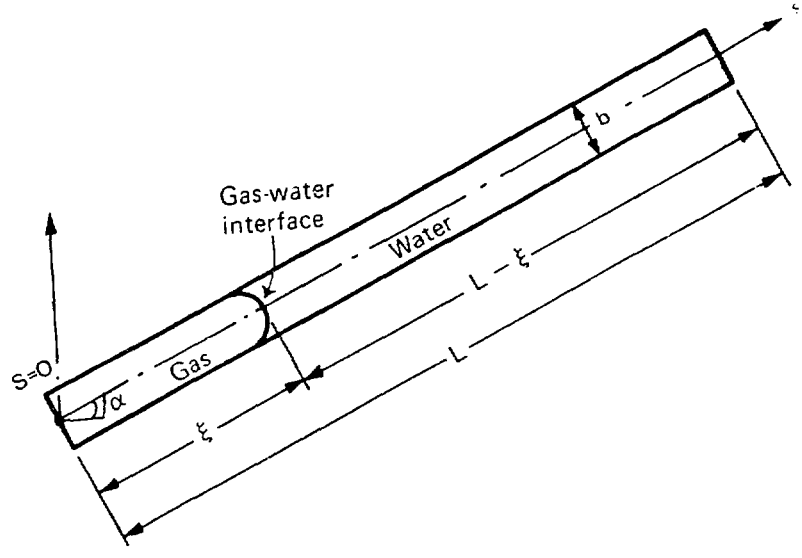

FIGURE B-2: Sketch for the Nomenclature for Gas-Water Displacement

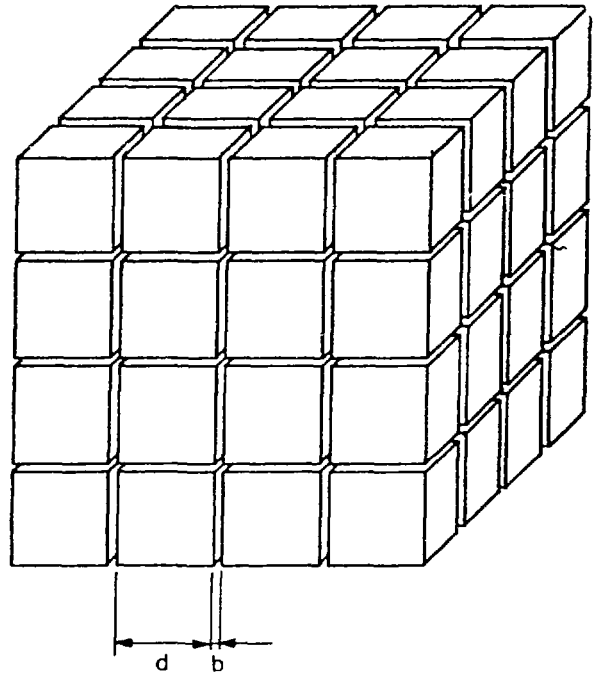

FIGURE B-3: An Idealized Representation of a Fractured Rock

ISSN 0067-0367

To identify individual documents in the series we have assigned an AECL— number to each.

Please refer to the AECL— number when requesting additional copies of this document from

Scientific Document Distribution Office
Atomic Energy of Canada Limited
Chalk River, Ontario, Canada
K0J 1J0

Price: B

ISSN 0067-0367

Pour identifier les rapports individuels faisant partie de cette série, nous avons affecté un numéro AECL— à chacun d'eux.

Veuillez indiquer le numéro AECL— lorsque vous demandez d'autres exemplaires de ce rapport au

Service de Distribution des Documents Officiels
Energie Atomique du Canada Limitée
Chalk River, Ontario, Canada
K0J 1J0

Prix: B